Spatial and temporal distribution of seismicity along the northern Mid-Atlantic Ridge (15°-35°N)

Deborah K Smith, Javier Escartin, Mathilde Cannat, Maya Tolstoy, Christopher G Fox, Delwayne R Bohnenstiehl, Sara Bazin

Spatial and temporal distribution of seismicity along the northern Mid-Atlantic Ridge (15°–35°N)

Deborah K. Smith,[1] Javier Escartin,[2] Mathilde Cannat,[2] Maya Tolstoy,[3] Christopher G. Fox,[4] DelWayne R. Bohnenstiehl,[3] and Sara Bazin[2]

Received 8 May 2002; revised 16 September 2002; accepted 8 November 2002; published 25 March 2003.

[1] A detailed investigation of the relationship between the spatial and temporal patterns of the seismic activity recorded by six autonomous hydrophones and the structure of the northern Mid-Atlantic Ridge between 15° and 35°N is presented. Two years of monitoring yielded a total of 3485 hydroacoustically detected events within the array recorded by four or more hydrophones. The seismically active zone extends ~20 km to either side of the ridge axis, consistent with earlier results from studies of fault morphology. Along the axis, hydrophone-recorded activity shows important variations. Areas with intense and persistent seismic activity (stripes) stand in sharp contrast to areas that lack seismicity (gaps). The regions of persistent activity are a new observation at mid-ocean ridges. In general, the patterns of seismically active/inactive regions are also recognized in the 28-year teleseismic record, implying that these patterns are maintained at timescales between a few years and a few decades. We find no simple relationship between individual segment variables (e.g., length or trend of the segment, maximum offset of discontinuities, or along-axis change in mantle Bouguer anomaly (MBA) and water depths) and number of hydrophone-recorded events. There does appear to be a correlation between axial thermal structure and seismicity. Regions of low and high numbers of events would thus correspond to thinner (hotter) and thicker (colder) lithosphere, respectively. Seismicity may reflect thermal structure at short timescales (decadal or longer), while relief and inferred crustal thickness may integrate this structure over longer periods of time (order of 1 Myr). *INDEX TERMS:* 3025 Marine Geology and Geophysics: Marine seismics (0935); 3035 Marine Geology and Geophysics: Midocean ridge processes; 3040 Marine Geology and Geophysics: Plate tectonics (8150, 8155, 8157, 8158); 7220 Seismology: Oceanic crust; 8164 Tectonophysics: Stresses—crust and lithosphere; *KEYWORDS:* earthquakes, hydrophones, Mid-Atlantic Ridge, mid-ocean ridges, seismicity

Citation: Smith, D. K., J. Escartin, M. Cannat, M. Tolstoy, C. G. Fox, D. R. Bohnenstiehl, and S. Bazin, Spatial and temporal distribution of seismicity along the northern Mid-Atlantic Ridge (15°–35°N), *J. Geophys. Res.*, *108*(B3), 2167, doi:10.1029/2002JB001964, 2003.

1. Introduction

[2] In January 1999, six autonomous hydrophones, designed and built by NOAA's Pacific Marine Environmental Laboratory (PMEL), were moored on the flanks of the Mid-Atlantic Ridge (MAR) (Figure 1) to monitor the seismicity of a portion of this slow spreading ridge [*Smith et al.*, 2002]. Here we present a detailed look at the seismicity of the northern MAR between 15° and 35°N as recorded by the hydrophones for a period of ~2 years.

[3] The region of the MAR within the hydrophone array is part of the French American Ridge Atlantic (FARA) project, which extends from 15° to 40°N. This section of the MAR has been subject to intensive study over the past several years. Multibeam bathymetry data have been collected along the entire length of the ridge axis, and several surveys have extended well off axis [e.g., *Cannat et al.*, 1999; *Gente et al.*, 1995; *Needham et al.*, 1991; *Patriat et al.*, 1990; *Rommevaux et al.*, 1994; *Sempéré et al.*, 1995; *Thibaud et al.*, 1998; *Tucholke et al.*, 1997]. The FARA region includes several sites of multidisciplinary study. Well-known examples of which include the MARK area near 23°N [e.g., *Karson et al.*, 1987], the TAG hydrothermal vent field near 26°N [e.g., *Kleinrock and Humphris*, 1996b; *Rona et al.*, 1976], the segments between the Hayes and Oceanographer transforms (33°–35°N) [e.g., *Detrick et al.*, 1995], and the FAMOUS area near 37°N [e.g., *Heirtzler and van Andel*, 1977].

[4] There have been a number of detailed studies of teleseismic earthquakes on the MAR [e.g., *Bergman and*

[1]Woods Hole Oceanographic Institution, Woods Hole, Massachusetts, USA.
[2]Institut de Physique du Globe de Paris, Paris, France.
[3]Lamont-Doherty Earth Observatory, Palisades, New York, USA.
[4]National Oceanic and Atmospheric Administration/Pacific Marine Environmental Laboratory, Newport, Oregon, USA.

0148-0227/03/2002JB001964$09.00

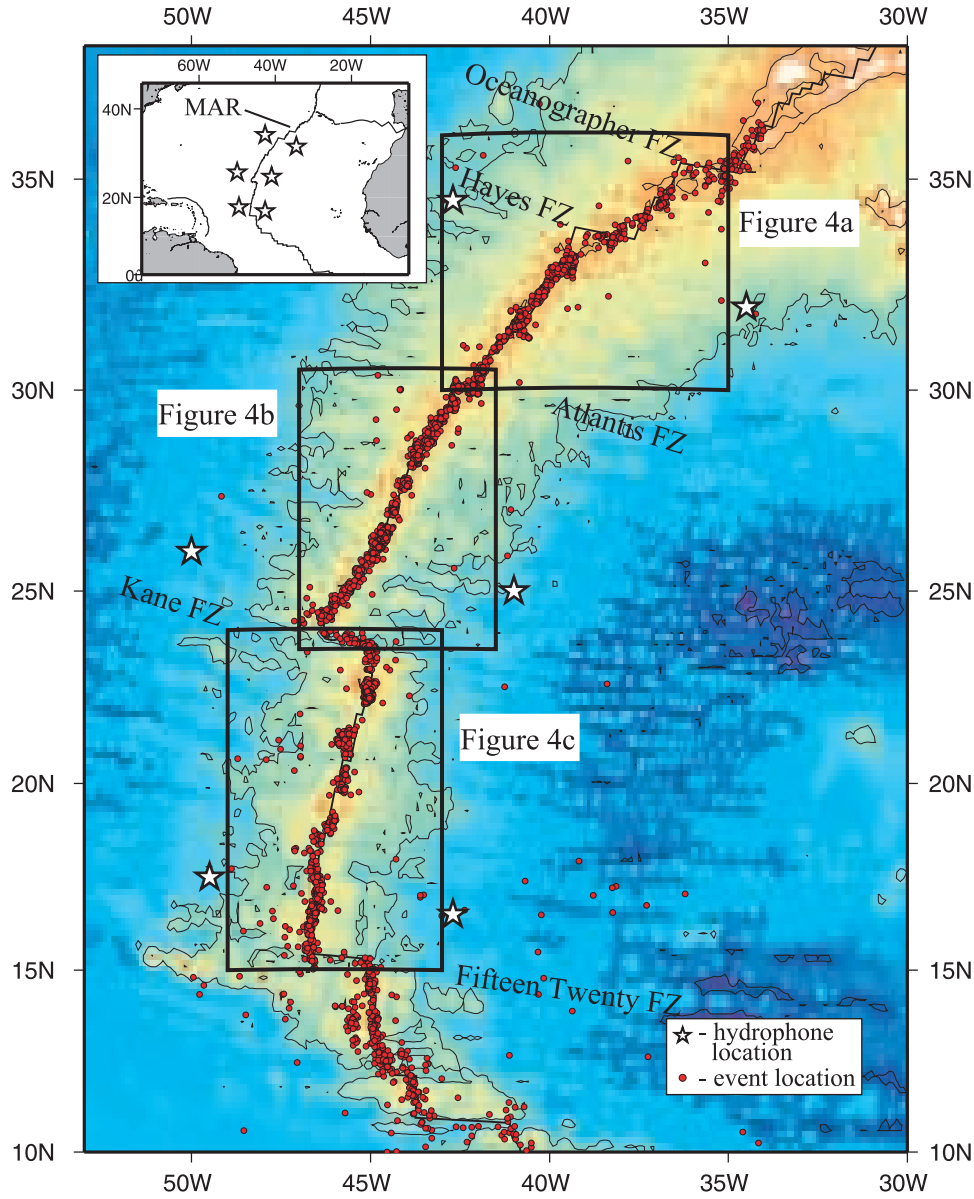

Figure 1. Map showing the location of the hydrophone array in the North Atlantic. Stars indicate the location of individual hydrophones. Red circles show the location of seismic events recorded by the hydrophone array during the first 554 days of deployment. A total of 4902 events were recorded within the Atlantic basin, and 3485 events were recorded within the hydrophone array by four or more hydrophones. Boxes mark the regions shown in Figure 4.

Solomon, 1990; *Huang and Solomon*, 1988; *Huang et al.*, 1986] and its fracture zones [e.g., *Abercrombie and Ekström*, 2001; *Wolfe et al.*, 1993]. In addition, a number of local microearthquake experiments using ocean bottom seismometers (OBS) have been conducted at various locations along the MAR [e.g., *Barclay et al.*, 2001; *Kong et al.*, 1992; *Toomey et al.*, 1985, 1988; *Wolfe et al.*, 1995]. All of these studies provide a framework within which we can place the results of the hydrophone monitoring.

[5] Results from the first year of hydrophone data allowed us to make some general observations on the seismicity [*Bohnenstiehl et al.*, 2000, 2002; *Smith et al.*, 2002]. The magnitude of completeness of the hydrophone data set is $m_c \sim 3.0$, with a number of smaller events being recorded. A significant variability in event rate along the axis of the MAR was observed within the array. Groups of neighboring segments appeared to behave similarly, producing an along-axis pattern with high and low levels of seismic activity. *Smith et al.* [2002] suggested that this broad-scale pattern is likely influenced by the axial thermal regime. In addition, data from off-axis indicated that most seismic faulting occurs within 15 km of the axis center. Finally, several earthquake sequences were detected that had variable temporal characteristics, suggesting fundamental differences in the causes of their seismicity [*Bohnenstiehl et al.*, 2000, 2002; *Smith et al.*, 2002].

[6] In this work we extend our study and present a detailed investigation of the relationship between the spatial

and temporal patterns of the seismic activity recorded by the hydrophones and the structure of the ridge, especially with regard to ridge axis segmentation. An additional year of data has been added. The ~2 years of monitoring (day 52, 1999, to day 78, 2001) yielded a total of 4922 hydroacoustic events from throughout the North Atlantic basin (0°–65°N, 60°W–20°W) recorded by four or more hydrophones. A total of 3485 of these events were located within the array (15°N–37°N, 50°W–34°W). This data set provides us with an unparalleled view of the seismicity of the ridge over a broad region and over a broad range of event magnitudes. The results are compared with recent teleseismic activity and with previous microearthquake studies within the study area. This comparison allows us to identify possible factors responsible for the observed patterns of seismicity and their variations along axis.

2. Background

2.1. Segmentation of the Spreading Axis at the Northern MAR

[7] The MAR between 15° and 35°N is a slow spreading (~12 mm/yr, average half rate), divergent plate margin typically marked by a 1.5–3 km deep, 15–30 km wide axial rift valley. Five major transforms offset the ridge within the hydrophone array (Fifteen-Twenty, Kane, Atlantis, Hayes, and Oceanographer; Figure 1). Between the transforms the ridge is divided into spreading segments whose ends are defined by nontransform offsets [e.g., *Sempéré et al.*, 1993; *Spencer et al.*, 1997]. The rift valley commonly contains an axial volcanic ridge that is considered to be the predominant site of volcanic activity [e.g., *Ballard and van Andel*, 1977; *Smith and Cann*, 1993]. On the basis of the sizes of the volcanic ridges that have been constructed on the valley floor [e.g., *Ballard and van Andel*, 1977; *Gente et al.*, 1991; *Smith and Cann*, 1993, 1999], large volumes of lava must be erupted at the northern MAR. Currently, we do not know how frequently magmatic events occur, whether they migrate along the axis, whether there are spatial patterns in these events, or how they vary through time.

[8] Faulting style is observed to vary along the length of a segment with faults having larger throws and wider spacing at segment ends than centers [e.g., *Mutter and Karson*, 1992; *Shaw*, 1992; *Shaw and Lin*, 1993]. Off axis elevated seafloor and residual gravity highs, and exposures of lower crustal/upper mantle rocks along the inside corners of ridge axis discontinuities suggest a cross-axis asymmetry in tectonic extension at slow spreading ridges [e.g., *Escartín and Lin*, 1995; *Severinghaus and Macdonald*, 1988; *Tucholke and Lin*, 1994], with most of the extension occurring at the inside corners. On the basis of the characteristics of fault populations there appear to be little, if any, faulting beyond the crest of the rift mountains (~1.5–3 Ma crust, typically 20–40 km from the axis [e.g., *Escartín et al.*, 1999]).

2.2. Seismic Studies at the Northern MAR

[9] As mentioned there have been a number of detailed studies of teleseismic earthquakes on the MAR [e.g., *Bergman and Solomon*, 1990; *Huang and Solomon*, 1988; *Huang et al.*, 1986]. The larger earthquakes occur preferentially in areas with a deeper median valley (generally segment ends) [*Huang and Solomon*, 1988], and are likely to be tectonic in origin. *Bergman and Solomon* [1990] concluded that volcanic earthquakes on the MAR probably fall below the magnitude threshold for teleseismic detection using global seismic networks. They observed a number of teleseismic swarms on the MAR, and determined that they were due to tectonic extension. The results of these studies, though, have been limited in their capacity to provide a representative account of general seismicity at the MAR, because they do not include the lower magnitude tectonic and volcanic events.

[10] Local microearthquake experiments have shown differing trends in seismicity for different MAR segments. For instance a progressive shoaling of events within the crust was observed toward the segment center at 26°N [*Kong et al.*, 1992], but that is not observed at 29°N [*Wolfe et al.*, 1995]. *Wolfe et al.* [1995] interpreted this as an indication that the thermal structure at the MAR is not in steady state. Therefore different styles of seismicity might be expected from segment to segment. Segment variability in microseismicity is corroborated by the study of *Barclay et al.* [2001], who found that the maximum depth of seismicity (3–4 km) at the center of the spreading segment near 35°N is anomalously shallow compared to other segments. *Barclay et al.* [2001] speculated that this is related to the thick crust and high crustal temperatures inferred for the center of the 35°N segment. Although not concurrent in time, these microearthquake studies help to constrain our interpretation of the hydrophone-recorded event patterns.

3. Hydrophone Data

[11] In order to monitor seismicity in remote areas of the world's oceans, PMEL developed autonomous hydrophone moorings. The hydrophones are able to record low-frequency acoustic energy in the Sound Fixing and Ranging (SOFAR) channel over extended periods. In 1996 PMEL moored six autonomous hydrophones in the equatorial Pacific and have been collecting data since then. On the basis of the success of the equatorial hydrophone array, in February 1999 six hydrophones were deployed in the North Atlantic. The Atlantic hydrophones are spaced ~1000 km apart and centered on the ridge axis (Figure 1). The data analyzed in this work were recorded between day 52, 1999, and day 78, 2001, and thus represent just over two years of monitoring.

[12] The hydrophone data are processed at PMEL as detailed elsewhere [*Fox et al.*, 2001]. The entire hydrophone earthquake database collected and processed to date is available on line at http://autochart.pmel.noaa.gov:1776/autochart/GetPosit.html. An example of the data is shown in Figure 2. The peak amplitude of the *T* wave signal packet is visually picked and used as the earthquake arrival time. After picking the events on individual hydrophones, PMEL software derives an event location, which includes its latitude, longitude, and source time; which of the hydrophones recorded the event; the estimated error for location and time; the acoustic magnitude at the source, and the error of that magnitude based on the variation of the estimates from each sensor.

[13] Acoustic magnitudes of oceanic earthquakes are estimated from the *T* wave signal amplitude by removing

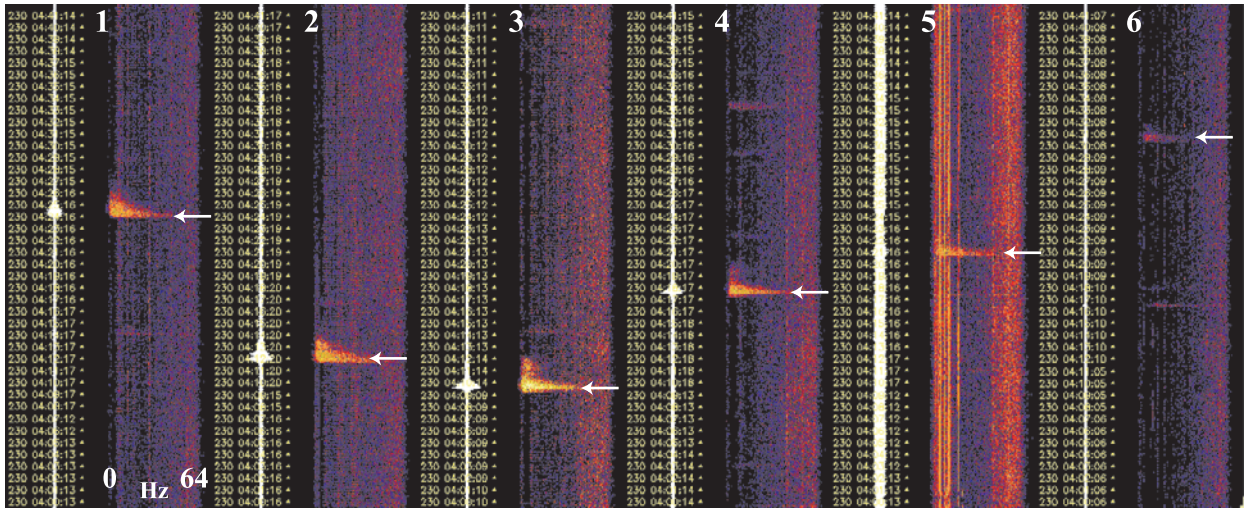

Figure 2. Display showing the time series and corresponding frequency spectra for an earthquake side by side. The earthquake was recorded by six hydrophones from the Atlantic array. Numbers mark the data from the six different hydrophones. Time stamps are shown along the time series data. The diagram shows several minutes of hydrophone time series data sampled at 128 Hz. The frequency spectra range from 0 to 64 Hz and were estimated from consecutive 1-s windows of the time series data. White arrows highlight the position of the *T* wave signals from this earthquake. Using the frequency spectra during routine earthquake processing allows for identification of *T* wave arrivals not readily apparent in the time series data. There are various periods of noise in the data including shipping noise, air gun surveys, possible navy sources, and possibly cable strumming in the case of the fifth hydrophone. The noise on this hydrophone is intermittent and generally does not interfere with the picking of arrivals, as seen on the figure.

the hydrophone instrument response and the transmission loss during propagation in the SOFAR channel. Only a very crude transmission loss estimate is used in routine processing, based on 5 km of spherical spreading following by simple cylindrical spreading with no bathymetric blockage. Although adequate for use in broad statistical analyses of the data [e.g., *Bohnenstiehl et al.*, 2000, 2002], acoustic magnitudes of individual events should be calculated with a full transmission loss model before being interpreted. Thus is this work we do not consider the magnitudes of events in our interpretations of segment-scale processes.

[14] Spectral amplitudes between 5 and 30 Hz are typically used to estimate acoustic magnitudes since this band provides the optimum *T* wave signal-to-noise ratio for magnitude >2 earthquakes [*Dziak et al.*, 1997]. The acoustic energy (power) levels of the earthquakes are determined by averaging the source level estimated from each hydrophone. The resulting magnitude represents the acoustic energy of the earthquake at the seafloor-water interface, and is in units of decibels (dB) relative to pressure (micropascals) at a reference distance of 1 m above the seafloor. All reference to dB in this paper will be similarly referenced.

[15] As discussed by *Fox et al.* [2001], T wave source location is the most accurate term for the locations derived from the hydrophone data because they mark where the energy leaves the seafloor and enters the water column. The locations may coincide with earthquake epicenters, but several other factors such as topographic relief, complex velocity structure of the crust, and depth of the earthquake below the seafloor may bias these locations. In some sections of the ridge, events are located both in the deepest parts of the valley floor as well as in the crestal mountains, which rise in some places to the depth of the SOFAR channel (~800–1000 m). Whether this indicates there is not a bias in the locations with respect to water depth, whether the events located at the tops of shallow features are topographically steered and epicenters are elsewhere, or whether the events on the deep parts of the valley floor are mislocated is impossible to know at this time.

[16] Predicted location errors within the array are based on the methods developed for the Pacific arrays [*Fox et al.*, 2001] using the Generalized Digital Environmental Model (GDEM) for the Atlantic and the hydrophone configuration shown in Figure 1. The error assumed for arrival times in the Pacific, based on the eruption at Loihi seamount off of the south coast of the Big Island of Hawaii, was standard deviation (SD) = 0.75 s. This error model accurately predicted the observed errors obtained in the least squares location analysis. Since there is no known volcanic point source in the Atlantic, a value for arrival pick error was inverted from the two years of earthquake locations. To match the prediction model accurately, the arrival time picking error for the Atlantic array had to be doubled to SD = 1.5 s. This increase in pick error for the Atlantic case is most likely due to differences in the geological setting (for example rougher seafloor or deeper source depths) that result in a broader, less impulsive *T* wave. The predicted location errors based on this higher arrival pick error are SD = ~2 km in latitude and longitude within the Atlantic array based on 972 events recorded on all six hydrophones. Using fewer hydrophones does not significantly change the error prediction, although the measured location errors become less dependable with fewer degrees of freedom.

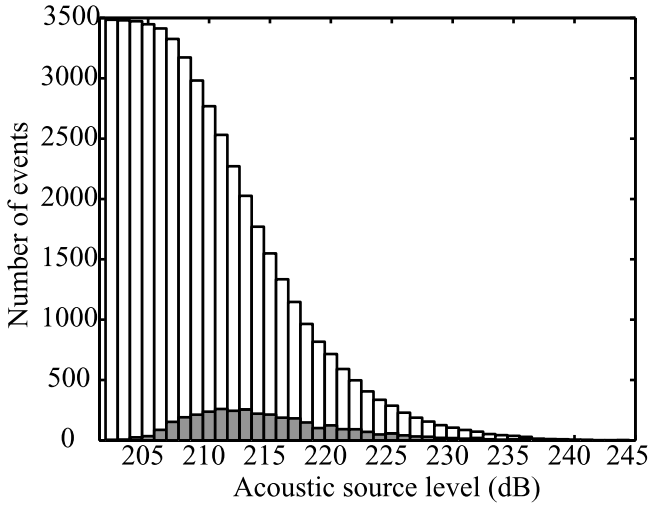

Figure 3. Histograms of the *T* wave acoustic source levels of earthquakes located from the data collected during the 2-year monitoring period. The events were all located within the hydrophone array, and only those events recorded on four or more hydrophones are included. The lower shaded histogram shows the number of events in 1-dB bins and indicates event detections are reliable to 208–210 dB. *T* waves are still recorded at <205 dB. The cumulative histogram is also shown and illustrates that more than 3000 events were recorded during the 2 years with acoustic magnitudes of 208 dB or greater, roughly 2 orders of magnitude more events than recorded teleseismically.

[17] Below a source magnitude of 208 dB, the number of earthquakes located from the hydrophones data falls off significantly, as can be seen on a plot of cumulative frequency versus magnitude (Figure 3). This indicates that events with acoustic magnitudes <208 dB may not be clearly recorded on four or more hydrophones due to variations in transmission loss within the array. Using the RAM propagation loss code [*Collins*, 1993, 1994] and the 5 Hz component of a hypothetical earthquake on the Hayes Fracture Zone at the northern end of the array, the predicted transmission loss to the nearest (northeast) hydrophone is ~100 dB. The transmission loss to the farthest (southwest) hydrophone is ~110 dB. On the basis of the Pacific model of *Fox et al.* [1999], this 10 dB difference is equivalent to more than 1 earthquake magnitude, but it does represents a "worst-case" geometry since much of the travel path runs along the crest of the shallow MAR. The predicted transmission loss to the southeast hydrophone is only ~104 dB, or ~0.5 magnitude difference from the northeast case. To minimize the bias from partially detected events, only events recorded on at least four hydrophones with acoustic magnitudes of ≥208 dB are used in the seismic analysis.

4. Data Analysis

[18] To investigate the spatial variability in hydrophone-recorded event rate along the axis of the MAR, we calculated the distance of each event along the axis from the Fifteen-Twenty Fracture Zone (FZ) using the finite pole of rotation (77.2°N, 76.3°E) determined for magnetic anomaly 3A by *Sloan and Patriat* [1992]. Bathymetry and gravity data were used to define the segmentation of the ridge axis within the hydrophone array. The results were based on published interpretations [*Sempéré et al.*, 1990; *Smith and Cann*, 1992; *Thibaud et al.*, 1998] and new information provided by multibeam bathymetry data collected during the hydrophone servicing cruises. Forty-five spreading segments have been identified between the Fifteen-Twenty and Oceanographer FZs (Table 1 and Figure 4). Of these 45 segments, 25 are "standard" MAR segments (indicated in Table 1), showing a shallower central region, a corresponding relative minimum in the gravity anomaly, and deeper extremities associated with relative gravity maxima [*Lin and Parmentier*, 1989]. The other 20 segments lack one or more of these characteristics.

[19] To examine the relationships between the spatial distribution of hydrophone-recorded events and ridge segmentation, we have assigned to each segment those events that have occurred within a box defined by flow lines passing 10 km to the north and south of the ends of the segment, and extending off axis to anomaly 3A (5.69 Myr). In cases of overlap, an event is assigned to the segment that is nearest to its location. To define this box, we have used the pole and angle of finite rotation given above [*Sloan and Patriat*, 1992]. This corresponds to spreading directions that vary between 104° and 101°, and spreading rates that vary between 22 and 24.9 mm/yr, from south to north (Fifteen-Twenty FZ to Oceanographer FZ).

[20] We also compare the 2-year pattern of hydrophone-recorded events with the longer term teleseismic pattern, and the more temporally and spatially restricted pattern of earthquakes recorded by OBSs. Teleseismic event locations and magnitudes were obtained from the National Seismic System composite catalog for the period 1973–2001. Because the coverage of the catalog is not uniform in time we restrict some of our comparisons to teleseismic events occurring between 1990 and 2000. Information on the microseismicity of the ridge axis was obtained from four regions within the hydrophone array where OBSs were deployed for periods of a few weeks or more. These regions are located along the axis of the MAR at ~22.5°N [*Toomey et al.*, 1988], 26°N (TAG) [*Kong et al.*, 1992], 29°N [*Wolfe et al.*, 1995], and 35°N [*Barclay et al.*, 2001]. Seismic moments of the OBS events were converted to body wave magnitudes for ease of comparison to teleseismic magnitudes.

[21] Using the method described above, we assign 2842 of the 3485 events within the array to the 45 segments identified (Table 1); all 2842 have acoustic magnitudes ≥208 dB. The same procedure is used for teleseismic events recorded between 1973 and 2001. Most of the hydrophone (87.7%, Figure 5) and the teleseismic events (84.2%) are located <20 km from the ridge axis, even with the larger errors associated with teleseismic locations.

5. Large-Scale Variability in Hydrophone-Recorded Events

5.1. Supersegments

[22] Within the hydrophone array the ridge can be divided into "supersegments": regions of the ridge bounded by the major fracture zones. Table 2 shows the number of hydrophone-recorded events normalized to a length of 100 km for

Table 1. Characteristics of Segments Within the Hydrophone Array[a]

	South End		North End									
Segment	Lat, °N	Lon, °W	Lat, °N	Lon, °W	Length, km	Az, °N	Off S, km	Off N, km	Depth,[b] m	Hyd	Tel	Comment
1	15.358	46.625	15.9	46.617	60.24	0.81	175.0	1.7	4300	36	22	
2	15.9	46.633	16.283	46.617	42.6	2.3	1.7	0.0	3600	41	6	
3	16.283	46.617	16.7	46.525	47.37	11.94	0.0	6.5	4000	106	26	
4	16.683	46.467	16.917	46.45	26.07	3.98	6.5	4.5	4700	24	6	
5[c]	16.95	46.475	17.508	46.425	62.24	4.89	4.5	9.6	3800	74	8	K11[d]
6	17.53	46.513	17.8	46.5	30.04	2.63	9.6	26.7	4500	17	10	
7[c]	17.917	46.72	18.517	46.617	67.56	9.26	26.7	28.2	3500	25	5	K10
8[c]	18.5	46.35	18.958	46.225	52.57	14.49	28.2	16.5	3700	29	5	K9
9[c]	18.983	46.07	19.308	46	36.86	11.5	16.5	0.0	3400	13	4	K8
10[c]	19.308	46	19.817	45.9	57.53	10.49	0.0	16.5	3300	8	3	K7
11[c]	19.817	45.742	20.397	45.642	65.29	9.2	16.5	6.1	4000	41	19	K6
12	20.4	45.7	20.967	45.683	63.04	1.61	6.1	10.4	3400	29	4	
13	20.975	45.783	21.397	45.742	47.09	5.18	10.4	40.8	4400	99	15	
14[c]	21.355	45.35	22.225	45.108	99.86	14.48	40.8	0.0	3000	22	11	K3
15	22.225	45.108	22.667	45.008	50.18	11.81	0.0	3.1	3900	229	28	
16[c]	22.667	44.978	23.15	44.925	53.95	5.77	3.1	1.7	3400	23	5	K2a
17	23.15	44.942	23.628	44.905	53.25	4.06	1.7	148.6	4300	87	26	
18[c]	23.85	46.345	24.45	46.208	68.11	11.77	148.6	0.0	4200	190	11	KA14
19	24.45	46.208	24.65	46.125	23.76	20.68	0.0	9.5	4200	9	2	
20	24.633	46.033	24.883	45.75	39.84	45.79	9.5	22.7	4400	49	10	
21	24.883	45.525	25.35	45.45	52.44	8.27	22.7	5.0	3500	49	8	
22	25.35	45.4	25.617	45.258	32.91	25.65	5.0	7.7	4100	47	4	
23	25.6	45.183	25.95	45.033	41.69	21.1	7.7	10.6	4200	33	10	
24	25.917	44.933	26.25	44.808	39.05	18.63	10.6	6.8	3800	68	7	
25[c]	26.233	44.742	26.625	44.625	45.09	14.96	6.8	4.3	3600	117	20	KA9
26[c]	26.6	44.592	26.908	44.492	35.64	16.17	4.3	0.0	3500	8	26	KA8
27	26.908	44.492	27.133	44.425	25.87	14.86	0.0	9.9	3900	54	8	
28[c]	27.167	44.333	27.733	44.067	68.15	22.64	9.9	2.4	3400	54	35	KA6
29[c]	27.717	44.05	28.2	43.895	55.79	15.83	2.4	6.1	3200	29	7	KA5
30[c]	28.2	43.833	28.677	43.607	57.43	22.62	6.1	8.2	3200	144	31	KA4
31	28.692	43.525	28.85	43.383	22.35	38.23	8.2	9.8	3800	61	13	
32[c]	28.842	43.283	29.408	43.083	65.83	17.15	9.8	17.5	3200	156	12	KA2
33[c]	29.367	42.908	30.117	42.7	85.73	13.54	17.5	69.2	3300	107	25	KA1
34	30.025	41.988	30.417	41.933	43.88	6.91	69.2	8.4	3800	68	15	
35	30.492	41.925	30.83	41.655	45.57	34.49	8.4	5.6	3400	23	16	
36[c]	30.8	41.608	31.192	41.35	50.02	29.43	5.6	8.4	3500	15	29	HA7
37[c]	31.167	41.267	31.75	40.753	81.07	36.95	8.4	9.3	3300	203	19	HA6
38[c]	31.717	40.663	32.267	40.242	72.87	32.99	9.3	15.8	3200	71	22	HA5
39	32.283	40.075	32.683	39.983	45.28	10.98	15.8	6.4	3200	44	9	
40[c]	32.667	39.917	33.12	39.475	65.08	39.33	6.4	21.2	3400	124	17	
41[c]	33.125	39.247	33.717	39.033	68.72	16.79	21.2	75.5	2300	51	5	HA1
42	33.583	38.233	33.717	38.133	17.53	31.85	75.5	32.4	3950	30	13	
43[c]	33.717	37.783	34.1	37.633	44.75	18.01	32.4	38.7	3100	27	6	OH3
44[c]	34.05	37.217	34.527	37	56.63	20.6	38.7	39.0	3100	80	42	OH2
45[c]	34.5	36.575	35.267	36.283	89.3	17.34	39.0	120.0	2200	28	23	OH1

[a]Az, azimuth; Off S, offset at south end; Off N, offset at north end; Hyd, number of hydrophone events; Tel, number of teleseismic events.
[b]Axial depth at segment center.
[c]"Standard" segments as defined in the text.
[d]Name of segment from *Thibaud et al.* [1998].

each supersegment for the two years of data. As described in the previous section, the numbers include all events on crust less than ~5.69 Myr (anomaly 3A). Regional ridge obliquity is also given in Table 2 and defined as the difference between the overall azimuth of the ridge section and the direction perpendicular to average spreading direction. The ridge obliquity in the four supersegments varies between 0° (Fifteen-Twenty to Kane), and 30° (Hayes to Oceanographer). The normalized number of teleseismic events for the 10-year period between 1990 and 2000 (and 1980 and 1990) is also given.

[23] Table 2 shows that the Kane to Atlantis supersegment had the highest normalized number of hydrophone-recorded events per 100 km in the 2 years of monitoring. This value includes a large earthquake sequence (165 aftershocks) that occurred in the rift mountains of segment 18 [*Bohnenstiehl et al.*, 2000, 2002]. Without that sequence, the number of hydrophone-recorded events/100 km is similar in the three supersegments between the Fifteen-Twenty and Hayes FZ. The Hayes to Oceanographer supersegment had the lowest number of hydrophone-recorded events. Teleseismic events recorded over the past 10 years show a different pattern, with the number of events per 100 km increasing to the north instead of decreasing. Normalized numbers of teleseismic events for the previous 10 years (1980–1990; Table 2), however, show yet a different pattern, suggesting that there is no persistent difference in the frequency of large earthquakes between the four supersegments. In the period 1980–1990 the Hayes to Oceanographer supersegment was the least active teleseismically, similar to what is observed from the hydrophone data (Table 2).

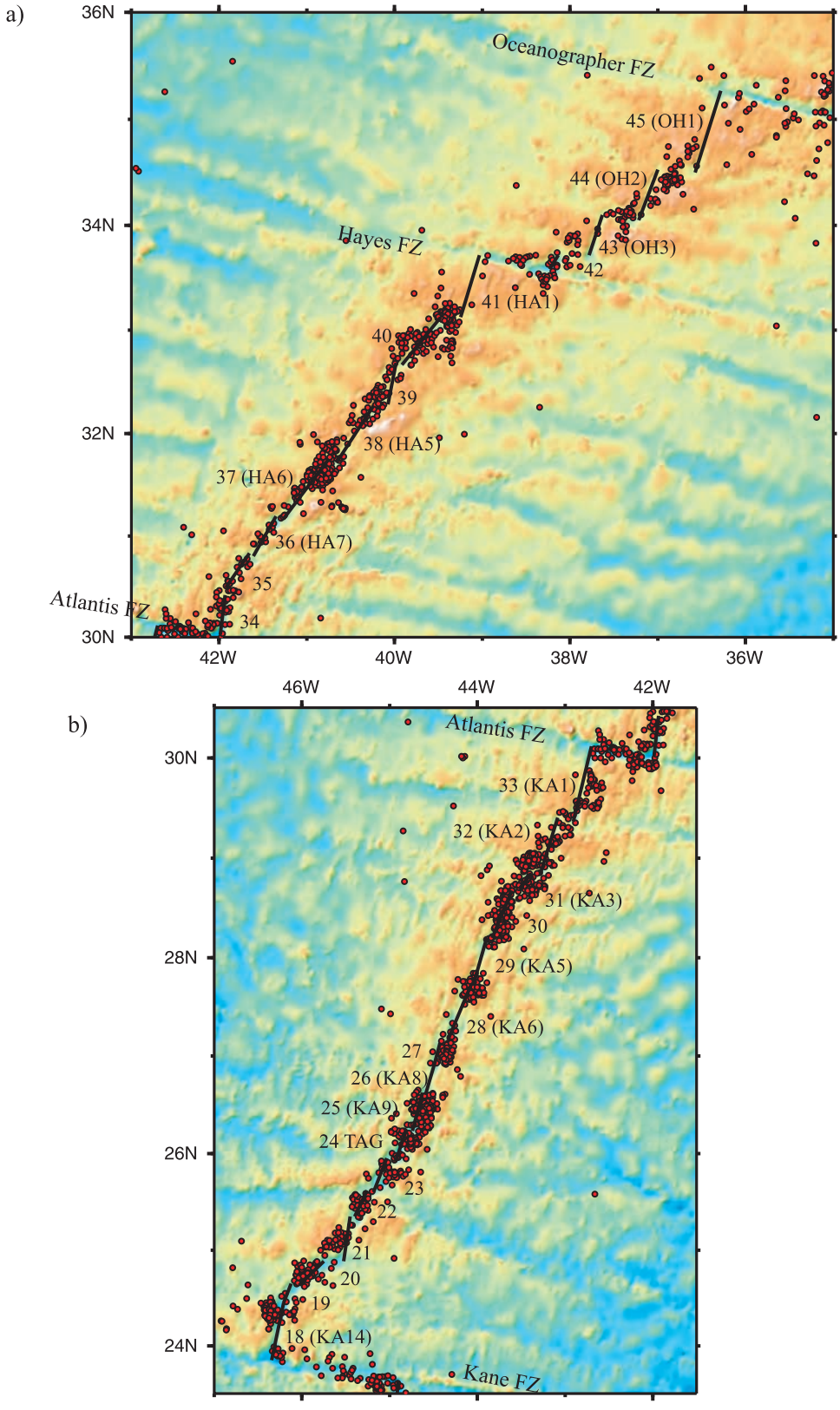

Figure 4. Location of hydrophone-recorded events (red circles) and bathymetry derived from satellite gravity data [*Smith and Sandwell*, 1997] of the region between (a) Atlantis and Oceanographer FZs, 30°–35°N; (b) Kane and Atlantis FZs, 24°–30°N; and (c) Fifteen-Twenty and Kane FZs, 15°–24°N. Segments are numbered starting at the Fifteen-Twenty FZ and correspond to those in Table 1. Note the striking gaps in seismicity along the axis especially between the Fifteen-Twenty and Kane FZs.

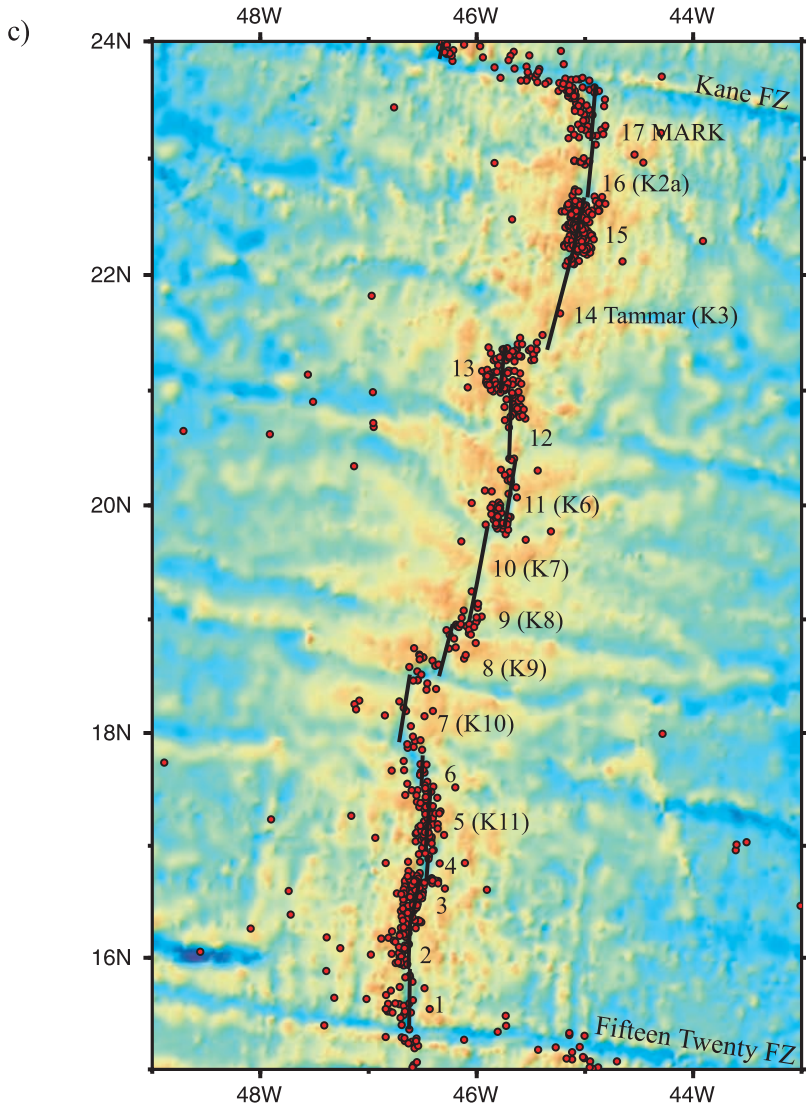

Figure 4. (continued)

5.2. Seismicity Along Transform Faults

[24] The major transform faults associated with the Oceanographer, Hayes, Kane, Atlantis, and Fifteen-Twenty FZs show differing amounts of seismic activity during the two years of hydroacoustic monitoring (Figures 4 and 6). The Kane and Atlantis transform faults were active. In contrast, the Fifteen-Twenty, Hayes, and Oceanographer transforms showed little seismic activity. A seismic moment deficiency has been observed teleseismically along oceanic transform faults [e.g., *Brune*, 1968; *Engeln et al.*, 1986; *Abercrombie and Ekström*, 2001]. The lack of hydroacoustically recorded seismicity along some of the transforms suggests that the seismic deficit may not be accounted for by a high number of smaller-magnitude earthquakes. Instead the lack of seismicity may indicate that aseismic slip occurs. This is consistent with the presence of serpentinite, which displays stable sliding (velocity strengthening behavior) for velocities consistent with those expected along slow spreading transform faults [*Reinen*, 2000; *Reinen et al.*, 1994].

5.3. Along-Axis Variability in Seismicity: Stripes and Gaps

[25] Within the hydrophone array, along-axis event rate shows an uneven distribution (Figure 6), with zones that are seismically inactive (gaps) and areas that have shown continuous seismic activity throughout the two years of monitoring (stripes). Gaps, defined as regions with less than five hydrophone-recorded events in 0.1° bins along the axis, must correspond either to areas where deformation is accommodated through low magnitude seismicity (lower than the detection limit of the hydrophone array) or to areas where deformation occurs aseismically, or to quiescent areas in which stress is accumulating and not being released [e.g., *Arnott and Foulger*, 1994].

[26] Eleven conspicuous stripes (areas of continuous activity as seen in the right panel of Figure 6) are identified, two of which correspond to the Kane and Atlantis transform faults. The other nine stripes correspond to areas with large numbers of events (Table 1). The segments within which the stripes occur are marked on Figure 6, the most prominent

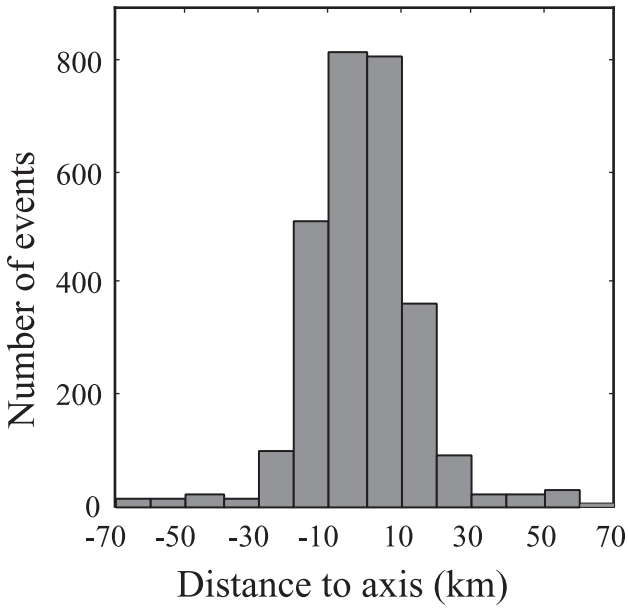

Figure 5. Number of hydrophone-recorded events versus distance to the ridge axis (negative distances are to the west). Total number of events is 2842.

being in segments 13 and 15. Note that the teleseismic events that occurred within the monitoring period do not appear to trigger the activity in the stripes.

[27] The pattern of seismically active/inactive areas observed in the hydrophone data can be recognized in the longer-term teleseismic record (data from 1973 to 2001), although it is not as clearly defined. This lack of definition may be due to the lower number of events (648 teleseismic events, Figure 6), and perhaps the much larger error ellipses associated with teleseismic locations. The similarities suggest that the patterns of seismicity along the axis can be persistent at timescales of 1 year to a few decades.

5.4. Along-Axis Variability in Seismicity: Variability Between Segments

[28] To compare the level of seismicity between individual segments, the number of hydrophone-recorded events in each segment (Table 1) has been normalized to an average segment length of 40 km. The normalized number of hydrophone-recorded events varies between 5.5 (segment 10) and 182.5 (segment 15) for the 2-year deployment. Figure 7 shows that the normalized number of hydrophone-recorded events is <40 in 25 out of the 45 segments. The gaps in seismicity, as labeled on Figure 6 occur within these segments that have low normalized number of events. Stripes occur within segments that have normalized numbers of hydrophone-recorded events >75. There are segments with low and high number of events that are not gaps and stripes. In these segments, the events are either clustered in time or spatially diffuse. For example, in the case of segment 18 as mentioned above, the magnitude 5.9 normal faulting event along the rift valley wall in April 1999 was followed by 165 aftershocks [*Bohnenstiehl et al.*, 2000, 2002; *Smith et al.*, 2002], with a rapid decay in seismic activity, following an Omori's Law [*Utsu et al.*, 1995].

[29] The number of teleseismic events per segment for the period 1973–2001, also normalized to a segment length of 40 km, varies between 2.1 (segment 10) and 29.7 (segment 44). Figure 7 shows that the normalized number of teleseismic events is <10 in 24 out of 45 segments. In general, the normalized number of hydrophone-recorded events within segments is positively correlated with the normalized number of teleseismic earthquakes recorded over the past 28 years. There are some significant exceptions to this, however. Segments 26 and 36 both have high rates of teleseismic activity, but have experienced only two and one teleseismic events, respectively, and <20 hydrophone-recorded events during the 2 years of monitoring.

[30] The supersegment between the Fifteen-Twenty and Kane FZs is dominated by segments with low levels of both hydrophone and teleseismic activity. This is especially striking in the region encompassing segments 7–10. Also in this supersegment, segment 15 stands out for its high normalized number of hydrophone and teleseismic events. It is the well defined stripe seen at ~775 km distance along the axis in Figure 6. Seismic activity was more or less continuous in segment 15 throughout the 2-year recording period with an average rate of 1 event/3 days. An OBS study was conducted by *Toomey et al.* [1988, 1985] at the northern end of the segment. We discuss the nature of this stripe in more detail in sections 7 and 8.

[31] Figure 8 shows that there is no clear relationship between the normalized number of hydrophone-recorded events in a segment, and the length or trend of the segment, the maximum offset of the discontinuities that bound the segment, or the contrast in MBA between segment ends and center. Many segments with a low normalized number of hydrophone-recorded events do, however, share two characteristics: they are "standard" segments (deeper extremities corresponding with gravity maxima, shallower center corresponding with gravity minima); and the axial depth at the segment center is ≤3700 m (Figure 9 and Table 3). All 11 segments that are associated with the gaps in seismicity marked on Figure 6 have an axial depth <3700 m at segment center (Figure 9 and Table 3), and only one of these segments is "nonstandard" (segment 12, which does not have a typically shaped MBA).

[32] Regional axial depths tend to shallow to the north of the study area, toward the Azores hot spot [e.g.,

Table 2. Characteristics of Ridge Sections Between the Major Fracture Zones

Regions bounded by FZs[a]	Length[b]	Obliquity, deg	Hydrophone Events, per 100 km	Teleseismic Events,[c] per 100 km
Hayes–Oceanographer (33–35°N)	220	30.3	73	28 (3)
Atlantis–Hayes (30–33°N)	453	21.5	127	15 (9)
Kane–Atlantis (24–30°N)	755	15.6	152	16 (9)
Fifteen-Twenty–Kane (15–24°N)	935	0	126	11 (6)

[a]For crust <5.69 Myr old.
[b]Projected to a great circle passing through pole of rotation.
[c]Numbers given for two time periods: 1990–2000 (1980–1990).

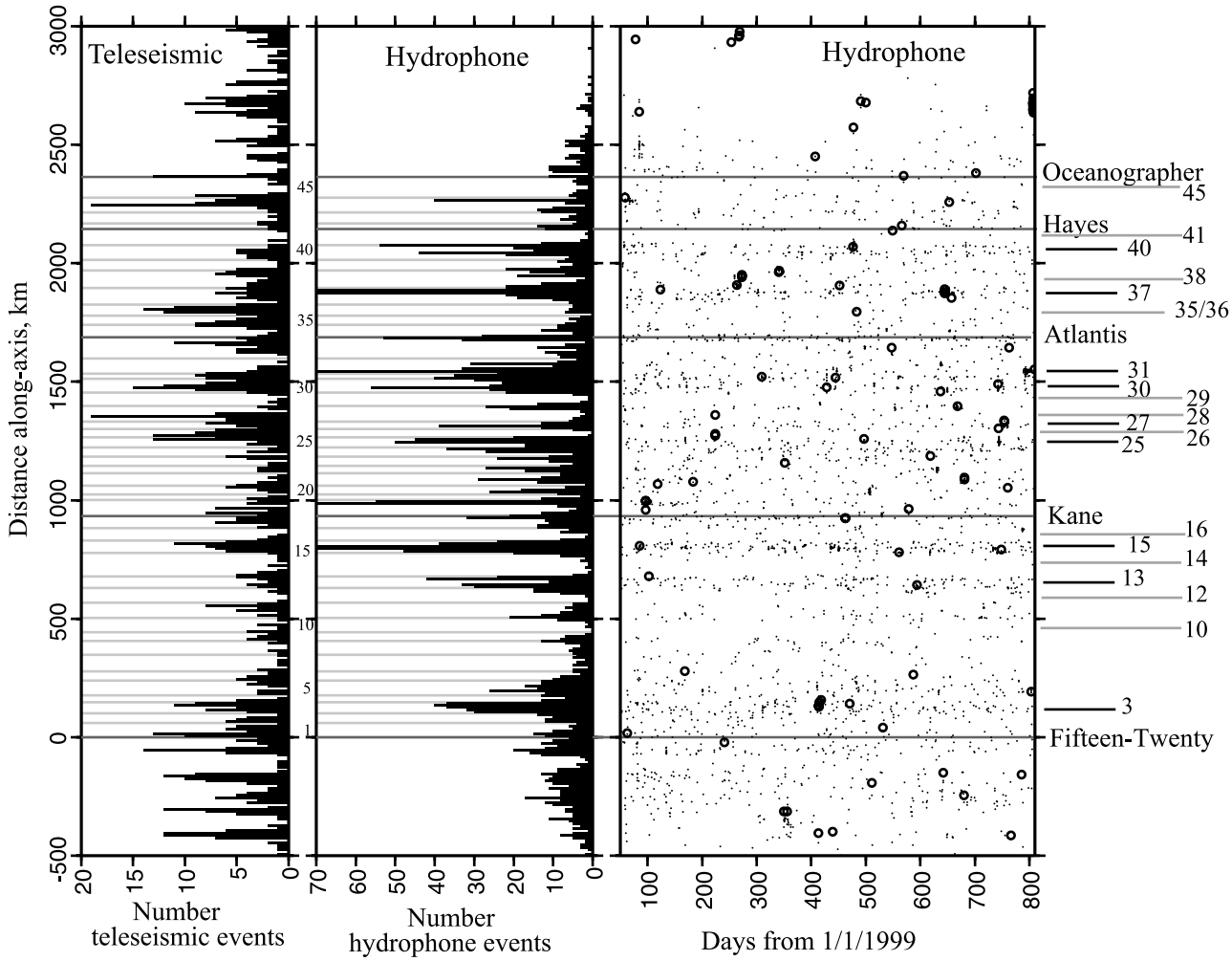

Figure 6. (left and middle) Histograms of distance along axis versus number of events for teleseismic and hydrophone source locations on crust <5.69 Myr old, 11 km (0.1°) bins: (left) 648 teleseismic events, (middle) 2842 hydrophone-recorded events, (right) 2842 hydrophone-recorded events plotted against deployment day starting from 1 January 1999. Light gray lines on Figures 6 (left) and 6 (middle) mark segment ends (Table 1). Segment numbers are shown between Figures 6 (left) and 6 (middle). Darker gray lines are FZs. Teleseismic events that occurred within the period of monitoring are shown as larger circles in Figure 6 (right). Note the presence of well-defined stripes of seismic events, indicating continuous seismic activity within a small area throughout the monitoring period. Stripes are marked to the right with black lines and labeled with the number of the segment within which they occurred. There are also gaps in the seismicity. These regions are marked on the right by gray lines and labeled with segment numbers. The marked gaps represent regions with less than five hydrophone-recorded events within the 2-year monitoring period.

Schilling et al., 1985]. Using the best fit line shown in Figure 9 lets us account for this systematic variation in depth, but using this line as a depth threshold instead of a depth of 3700 m does not modify the proportion of segments with shallow centers and a low level of hydrophone-recorded activity.

[33] Of the 20 segments with normalized number of hydrophone-recorded events >40 m (Figure 7 and Table 3), 11 are "nonstandard" segments with a segment center depth >3700 m, while 9 are "standard" segments with 7 of those having segment center depths <3700 m. Table 3 shows that the correspondence between the level of hydrophone-recorded activity (including stripes), segment morphology and gravity, and axial depth at segment center, is not as straightforward for segments with high hydrophone-recorded activity as those with low activity.

6. Segment-Scale Distribution of Hydrophone-Recorded Events

[34] The event locations we use correspond to the points where seismic energy radiates from the seafloor into the water column. These locations do not necessarily correspond to earthquake epicenters, and to what extent they can be used to determine small-scale variations in earthquake patterns is unknown. Nonetheless, we find there are systematic variations in the distribution of hydrophone-recorded events, and these are discussed below.

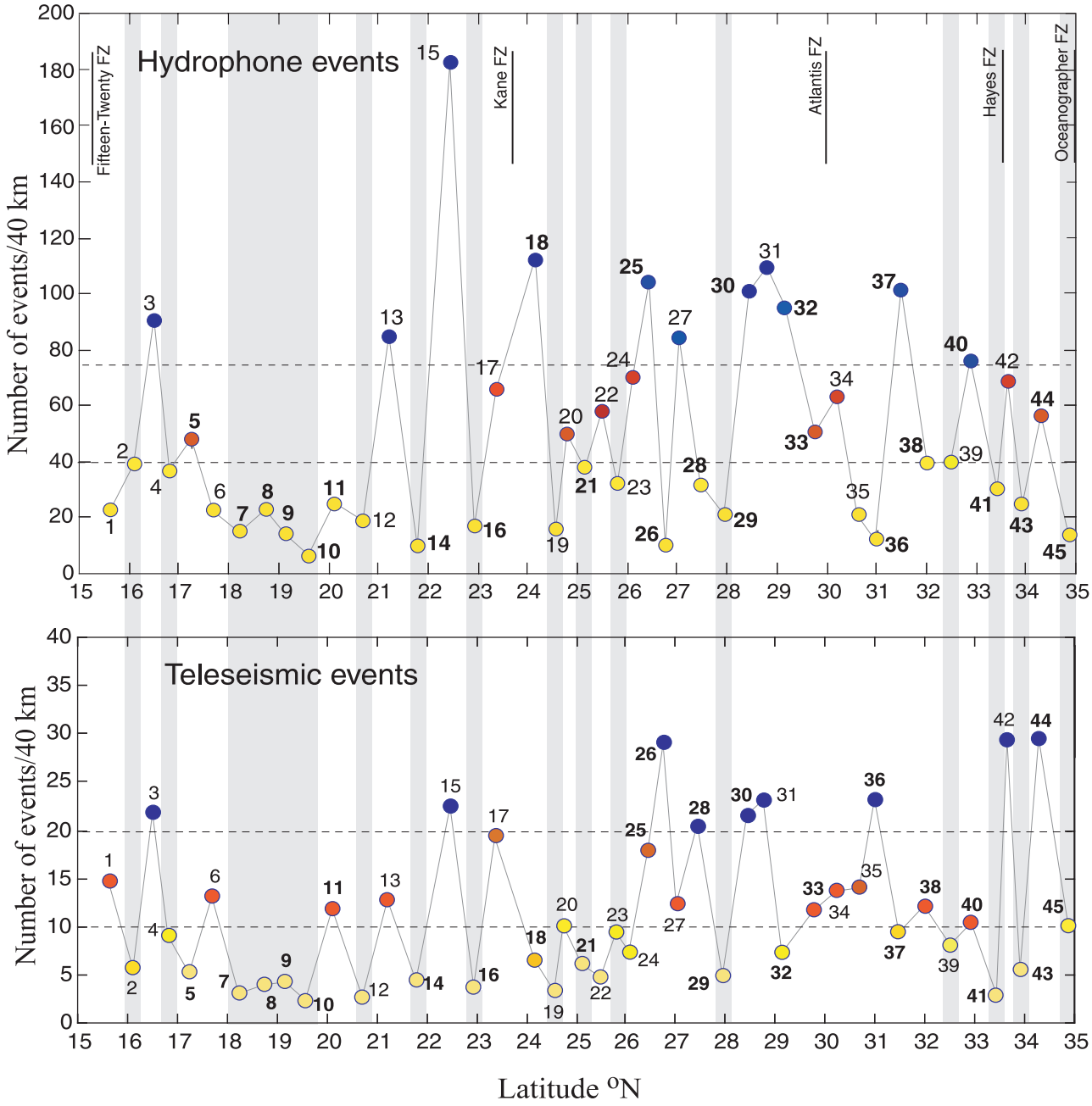

Figure 7. Number of events by segment, normalized to a segment length of 40 km: (top) hydrophone-recorded events and (bottom) teleseismic earthquakes (1973–2001). Dots indicate normalized number of earthquakes per segment. Horizontal lines are arbitrary and divide the segments into those with high (blue dots), medium (red dots), and low (yellow dots) event activity. Gray shading shows segments with low numbers of both hydrophone and teleseismic events. Standard segments are shown in bold.

[35] Most of the hydrophone-recorded events (79%) occur within 20 km of the segment ends (Figure 10a), and most segments are 40–70 km long (Table 1). This means that the center part (i.e., >20 km away from segment ends) is often shorter, if it exists at all, than the extremities (i.e.,<20 km away from segment ends). The high proportion of segment end events therefore, is largely due to the distribution of segment lengths in the study area. Figure 10b shows, however, that this trend of decreasing number of events with increasing distance to segment end persists when numbers of segment center events are normalized to a length of 40 km (equal to the combined length of the two segment ends). The proportion of segment end events is then 57.4%.

[36] The spatial distribution of hydrophone-recorded event locations across the ridge axis varies between segment centers and segment ends. The proportion of events located <10 km from the axis decreases from 67.5% at the segment center to 54.3% at the segment end, while events located between 10 and 20 km from the axis (over the rift mountains) is 20.6% for the segment center and 33.3% for the

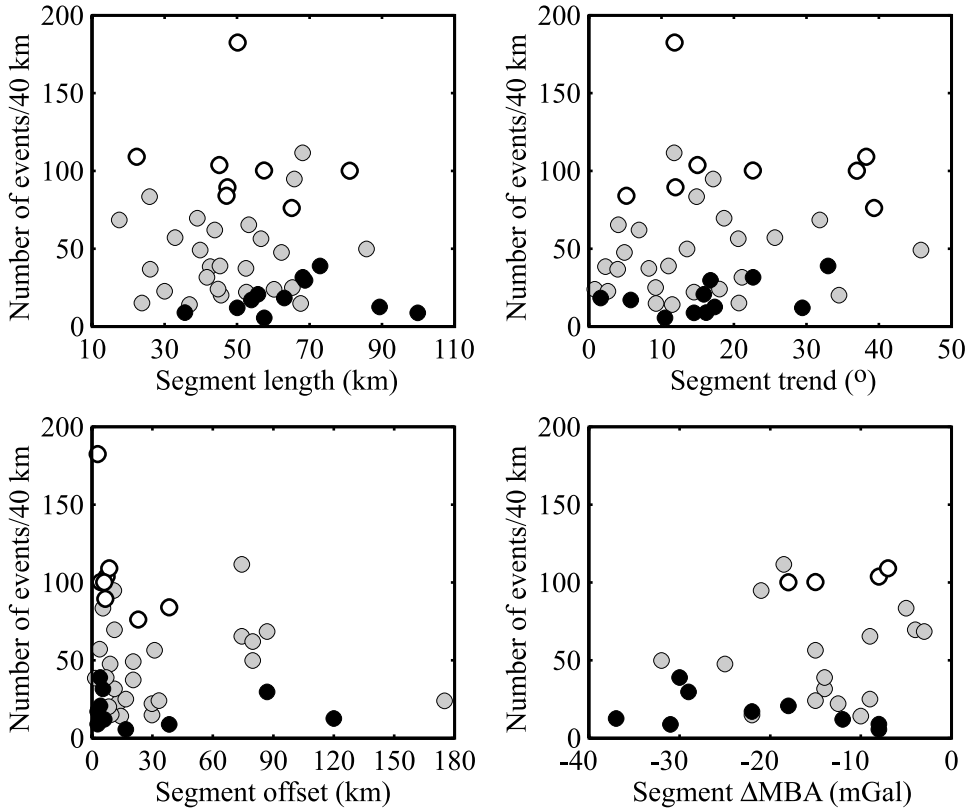

Figure 8. Number of hydrophone-recorded events per segment, normalized to a segment length of 40 km, as a function of different segment variables. (top left) Segment length. (top right) Segment trend (direction orthogonal to average spreading direction; zero obliquity is N12°). (bottom left) Maximum length of offset of discontinuities that bound the segment. (bottom right) Contrast in MBA between segment ends and segment center [*Thibaud et al.*, 1998]. Segments that correspond to the gaps in seismicity defined in Figure 6 (black dots) span a wide range of segment lengths, orientation, maximum offset, and along-axis MBA contrast. Open circles show segments containing stripes.

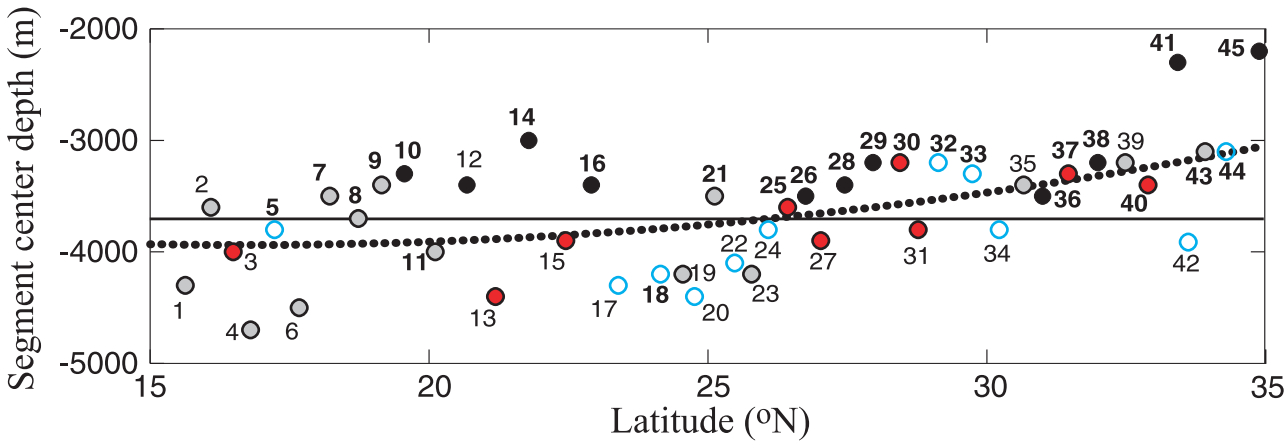

Figure 9. Axial depth at segment center as a function of latitude for the 45 ridge segments between the Fifteen-Twenty and Oceanographer FZs. Gray circles indicate segments with a normalized number of hydrophone-recorded events <40. Solid circles indicate gaps. Red circles indicate stripes. Blue circles indicate others. Solid line is 3700 m. Dotted line is best polynomial fit of the data, excluding segments 41 and 45 that stand out as particularly shallow. Axial depths tend to shallow to the north of the study area, toward the Azores hot spot. Twenty-five segments have <40 hydrophone-recorded events (55%); of these 19 have shallow axial depths. All segments with gaps have axial depths <3700 m.

Table 3. Stripes and Gaps

Segments	Total	Standard	Nonstandard	Shallow (<3700 m)[a]	Deep (>3700 m)[a]
<40 events[b]	25	18	7	16 (3)	2 (4)
Gaps within low event segments (10,12,14,16,26,28,29,35/36,38,41,45)	11	10	1	10 (1)	0
>40 events[c]	20	9	11	7 (0)	2 (11)
Stripes within high event segments (3,13,15,25,27,30,31,37,40)	9	4	5	4 (0)	0 (5)

[a]Numbers are given to identify standard and (nonstandard) segments.
[b]Segments 1,2,4,6,7,8,9,10,11,12,14,16,19,21,23,26,28,29,35,36,38,39,41,43,45.
[c]Segments 3,5,13,15,17,18,20,22,24,25,27,30,31,32,33,34,37,40,42,44.

segment end (Figure 11). Increased numbers of hydrophone-recorded event locations over the rift mountains of segment ends may, however, be influenced by the raised topography, which may act as a preferred radiator into the oceanic sound channel versus events generated from deeper locations which must propagate further before being entrained. We currently do not understand how important topographic steering is along this section of the MAR.

[37] The cross-axis spatial distribution of events also shows a marked asymmetry with more events occurring at inside corners (IC) than at the conjugate outside corners (OC), as was first observed in OBS studies [e.g., *Cessaro and Hussong*, 1986; *Rowlett*, 1981; *Rowlett and Forsyth*, 1984; *Wolfe et al.*, 1995]. To quantify this asymmetry, we define boxes that extend 20 km from the axis and from the discontinuity; the box on the active side of the discontinuity corresponds to the IC, while the box on the conjugate, inactive side corresponds to the OC. Only the 34 discontinuities with an offset >5 km (see Table 1) are used in the calculation. Although on average more events occurred at the IC (66.3%) than at the OC, the opposite pattern is observed in some of the segments (Figure 12).

7. Segments With OBS Studies

[38] Although the OBS studies we consider here are all limited in duration (a few to several weeks), we make the assumption that their results are representative of the longer term seismicity in these regions. We consider the geologic and geophysical characteristics of the four OBS segments (segments 45, 32, 24, 15) in detail (Table 4). Following *Thibaud et al.* [1998] each segment is categorized as "hot" or "cold," based on a combination of variables dependent on their thermal state. Hot segments show a strong change in along axis MBA and bathymetry, and a narrow inner valley, while cold segments have a smaller change in along-axis MBA and relief, and a wide inner valley floor. Additional information about crustal structure of each segment can be inferred from the shape of the along-axis profile taken along the top of the axial volcanic ridge, if one has been constructed, or the center of the segment otherwise [*Smith and Cann*, 1999]. *Smith and Cann* [1999] suggested, based on hydraulic potential arguments, that if magma reservoirs exist within the crust they must be located beneath the shallowest parts of the longitudinal profiles. If a profile comes to an abrupt peak, this would suggest that there is no magma reservoir within the crust or that it is small in its along-axis extent. If the shallowest part of the longitudinal profile is flat for some distance, then a magma reservoir (or at least a hydraulically connected magma system) could extend along the axis for as far as the crest is flat.

[39] Segments 45 and 32 (Table 4 and Figure 13) are hot segments and in our terminology are also standard, with depths at the bathymetric highs <3700 m, and bathymetric

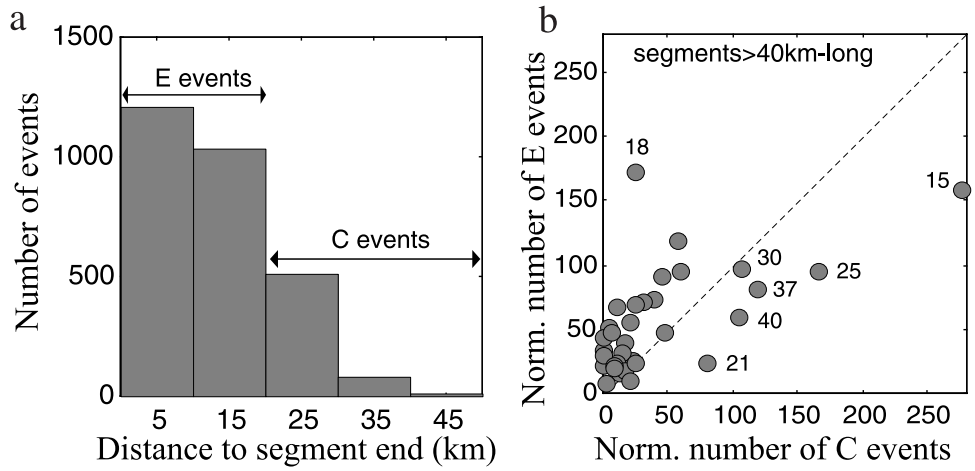

Figure 10. Segment-scale distributions of hydrophone-recorded events. (a) Number of events versus distance to segment ends. E events are events occurring <20 km from the segment end. C events are events occurring >20 km from the segment end. Total number of events is 2842. (b) Normalized number of E events versus normalized number of C events in segments >40 km long. Total number of events is 2462.

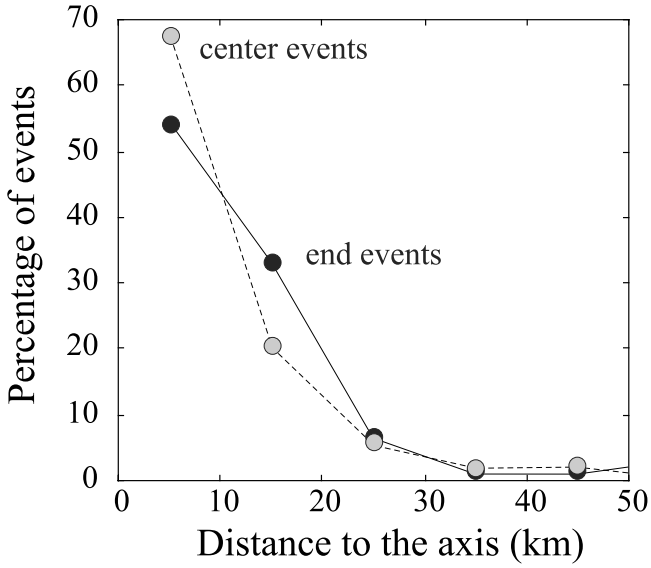

Figure 11. Number of segment end (solid dots and solid line) and of segment center (shaded dots and dashed line) hydrophone-recorded events in 10 km bins representing distance to the ridge axis. Total number of events is 2842. Seismicity continues farther from the axis at segment ends. Increased numbers of hydrophone-recorded event locations over the rift mountains of segment ends may, however, be influenced by the raised topography, which may act as a preferred radiator into the oceanic sound channel (see text).

profiles with flat tops of ~40 and ~20 km, respectively. Segment 32 has a large axial volcanic ridge built along much of its length, indicating that large volumes of lava have been erupted. The extent of the flat portion of the bathymetric profile suggests that a crustal magma reservoir may have extended (or extends) along much of the length of segment 32. The bathymetric profile of segment 45 has a shorter flat portion suggesting that crustal reservoirs may be restricted to the center of the segment. Segment 45 displays the greatest along-axis change in MBA and shallowest water depth of the four segments (Table 4), and recent looking lava flows have been observed at its center [*Bideau et al.*, 1998]. A shallow low-velocity body has been inferred 1–2 km beneath a volcano sitting near the segment center [*Barclay et al.*, 1998], and a chain of large seamounts extends to either side of the segment center [*Rabain et al.*, 2001]. All indications are that magma emplacement is greatly enhanced at the center of segment 45.

[40] Segments 24 and 15 are cold segments and non-standard, with depths at the along axis bathymetric high >3700 m (Figure 9 and Table 4). The profiles along segments 15 and 24 are sharply peaked with flat tops limited to ~7 km and ~15 km, respectively. If magma reservoirs reside within the crust at these segments they are likely limited in along-axis extent.

[41] In segment 45, the few events recorded by the hydrophones are located at the IC regions (Figure 13a). *Barclay et al.* [2001] reported on a microearthquake experiment conducted here. The OBS array was deployed at the center of the

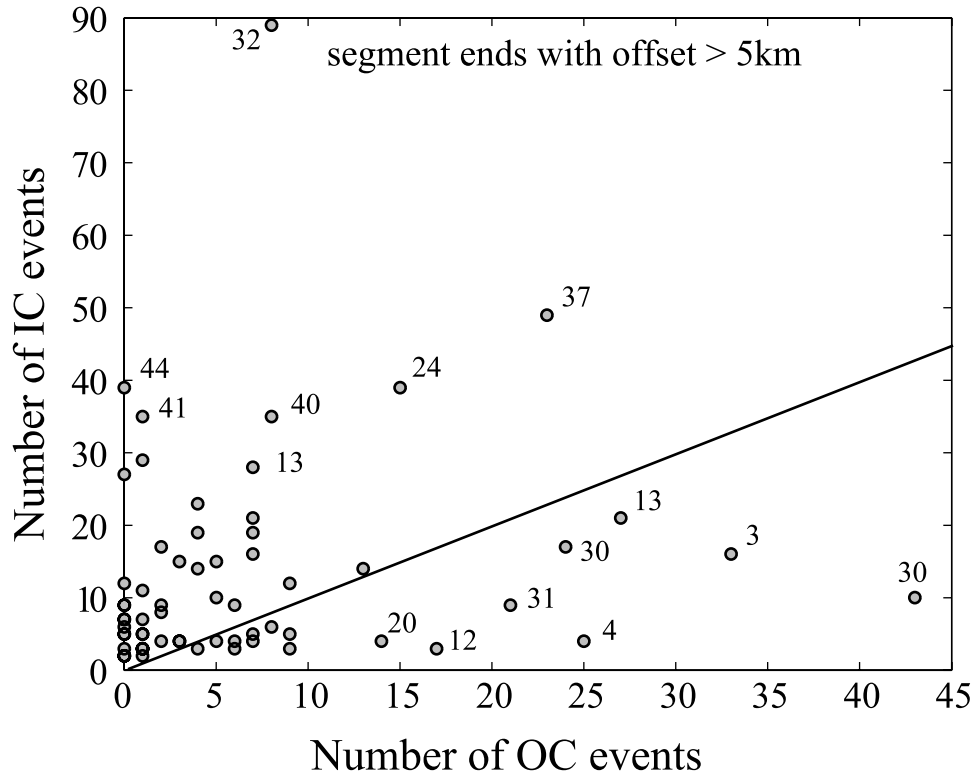

Figure 12. Number of inside corner (IC) versus outside corner (OC) hydrophone-recorded events in the 68 segment ends that abut discontinuities with offset >5 km. Total number of events is 1251. Number of IC events is more than the number of OC events in 51 of the 68 segment ends taken into account.

Table 4. Segments With Microearthquake Studies

Segment	ΔMBA	ΔR[a]	Normal Number of Hydrophone Events	Designation[b]	Flat Top of Long-Axis Bathymetry Profile	OBS Study	Interpretations
45 (OH1)	−37	1300	12	hot	20 km	*Barclay et al.* [2001]	hot regions beneath axis, in magmatic stage
32 (Broken Spur)	−21	600	94	hot	40 km	*Wolfe et al.* [1995]	brittle/ductile transition does not shallow toward center
24 (TAG)	−4	300	64	cold	15 km	*Kong et al.* [1992]	hot body beneath bathymetric high
15	–	500	183	cold	7 km	*Toomey et al.* [1985, 1988]	amagmatic for $\sim 10^4$ years

[a]Change in along-axis relief from segment end to center.
[b]From *Thibaud et al.* [1998].

segment, but earthquake locations were obtained along its entire length. Microearthquakes were recorded at the two inside corners (consistent with the results from the hydrophone data locations) and at the center of the segment. The maximum focal depth of the microearthquakes at the segment center was estimated to be ∼4 km, which is shallower than that obtained for other MAR segments where microearthquake studies have been conducted [*Barclay et al.*, 2001]. It is inferred from this that the brittle/ductile transition is shallow, and crustal temperatures are elevated at the center of segment 45. There have been no teleseismic events near the segment center in the last 27 years. Microearthquake magnitudes estimated for the center events are almost all <1. This magnitude is below the sensitivity of the hydrophones and well below that of the teleseismic network. No magnitudes are available for the IC microearthquakes for comparison.

[42] A microearthquake study at segment 32 (Broken Spur [*Murton et al.*, 1999]) covered the southern half of the segment [*Wolfe et al.*, 1995]. The greatest level of microearthquake activity was located on the southern inside corner (Figure 13b). The maximum depth of events located on the inner valley floor was more or less constant along the segment, and it was inferred that the brittle-ductile transition does not shoal from the end to the center of the segment. Nonetheless, variables such as the MBA [*Lin et al.*, 1990] and bathymetry indicate that the center of segment 32 has thicker crust or hotter mantle temperatures than the ends. *Wolfe et al.* [1995] suggested that the thermal structure of a segment may not be in steady state, and consequently the constant focal depths may indicate that segment 32 is cooling. This change in the thermal structure may not yet be reflected in the MBA and bathymetric profile.

[43] The spatial patterns of the hydrophone-recorded events in segment 32 are similar to the OBS patterns (Figure 13b): hydrophone-recorded events dominate the southern inside corner high, while only a small percentage are located near the segment center. Note that the hydrophone-recorded events are shifted to the west from the location of the microearthquakes at the IC and to the east at the segment center. This could be real or it could reflect topographic steering with energy radiating from shallower topography. Magnitudes of some of the microearthquakes are >2 at both the end of the segment and the center of the segment [*Wolfe et al.*, 1995], perhaps explaining why the hydrophones detected events in the center of this segment and not in segment 45.

[44] Segment 24 contains the TAG hydrothermal vent field near 26°N [e.g., *Kleinrock and Humphris*, 1996b; *Rona and Speer*, 1989] (Figure 13c). An OBS array centered on the axial bathymetric high covered about two thirds of the segment length [*Kong et al.*, 1992]. *Kong et al.* [1992] inferred that a recent magmatic intrusion was centered beneath the bathymetric high, extending southward ∼10 km, and coinciding with the flat portion of the bathymetric profile. The low-velocity region was thought to be relatively hot crust rather than molten material, and associated seismicity was interpreted as being triggered by cooling. Hydrophone-recorded events are located near the segment center where the largest magnitude microearthquakes (>1.5) were recorded. The hydrophone-recorded events are scattered across the bathymetric high into the nearby rift mountains (Figure 13c). As in segment 32 the hydrophone-recorded events in the rift mountains of segment 24 appear to be shifted to coincide with shallower topography. A teleseismic event occurred toward the end of the monitoring period in the eastern rift mountains at the southern end of the segment (Figure 13c) but lacked a typical aftershock sequence.

[45] Segment 15 contains a well-defined seismic stripe (Figure 6). An OBS array at the northern end of the segment [*Toomey et al.*, 1985, 1988] recorded numerous events extending from the northern end of the segment to near to the center, with focal depths of 4–8 km. The events were interpreted as tectonic in origin. The largest magnitude earthquakes (>2) recorded by the OBS array were located close to the center of the segment. On the basis of these results, *Toomey et al.* [1988] suggested that spreading has been accommodated by faulting at this segment for at least the last 10^4 years, implying that segment 15 is in an amagmatic phase. The hydrophone data show that the entire length of the segment was active during the two years of monitoring. As in other segments, there appears to be a shift in the hydrophone locations compared to the microearthquakes near the segment center and the northern end of the segment.

[46] Segment 15 has experienced a large number of teleseismic events in the last 28 years (Figure 13d). Three teleseismic events occurred during the hydrophone monitoring period, though none of them had a typical aftershock sequence [*Bohnenstiehl et al.*, 2000, 2002]. One of the teleseismic events was located in the rift mountains just to the west of the axial high, and the other two were located ∼10 and ∼20 km south of the high.

[47] Segments 15 and 24 are similar in many ways: very small or ambiguous ΔMBA, peaked bathymetric profile, teleseismic events during the deployment. In addition, they are both nonstandard segments with axial depths >3700 m. They are different in that segment 15 has a high number of hydrophone-recorded events while segment 24 has an intermediate number (Table 4). It is intriguing to think that segment 15 may be a snapshot of the TAG segment in

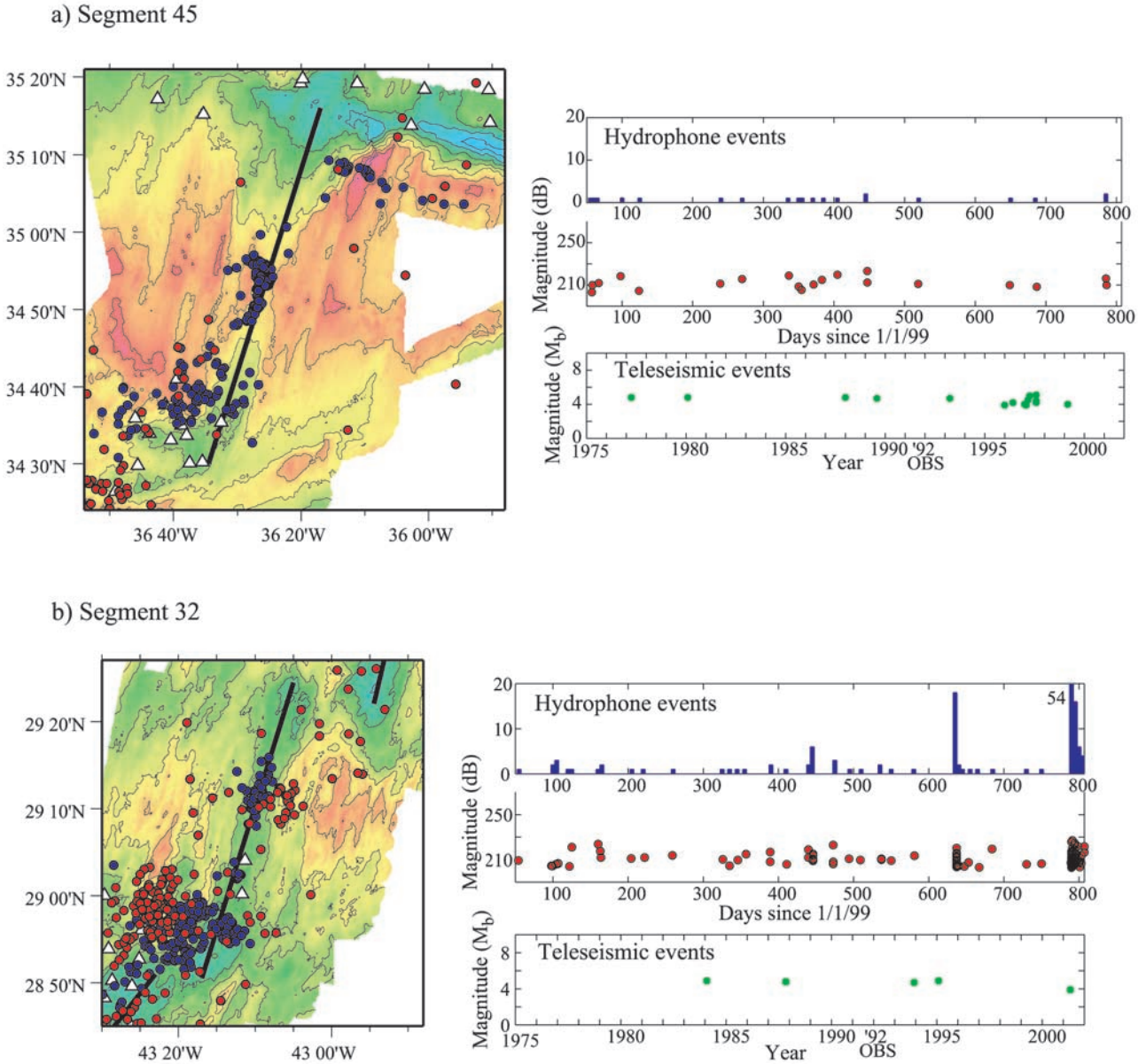

Figure 13. (a) Segment 45 near 35°N; (b) segment 32 near 29°N; (c) segment 24 (TAG) near 26°N; and (d) segment 15 near 22.5°N. Each shows the bathymetry of the area contoured at 200 m intervals. The ridge axis is marked by a solid dark line. Red circles are hydrophone-recorded events; blue circles: OBS events; white triangles are teleseismic events for the last 25 years. Panels show time series of the hydrophone and teleseismic data sets. (top and middle) Number and source levels of hydrophone data plotted as a function of days since 1 January 1999. Green circles show teleseismic events that occurred during the monitoring period plotted at an arbitrary acoustic magnitude of 240 dB. (bottom) Magnitudes of teleseismic events over the last 25 years. Where magnitudes of events are unknown they are plotted as zero. In Figure 13c the white cross marks the location of the TAG hydrothermal mound [e.g., *Kleinrock and Humphris*, 1996a].

an active tectonic stage. This is discussed in more detail below.

8. Discussion

8.1. Controls on Low Levels of Hydrophone-Recorded Event Rate

[48] There appears to be no simple correlation between individual segment variables and normalized number of hydrophone-recorded events (Figure 8). However, when variables are considered together patterns emerge. For example, considering *Thibaud et al.*'s [1998] hot and cold segments, defined from a combination of along-axis topography, water depth, and ΔMBA (all of which depend on the segments axial thermal structure), we find that their example of a cold segment (segment 31) has a high level of hydrophone-recorded activity, their examples of cold/intermediate segments (segments 44, 42, 39, 23, and 8) have

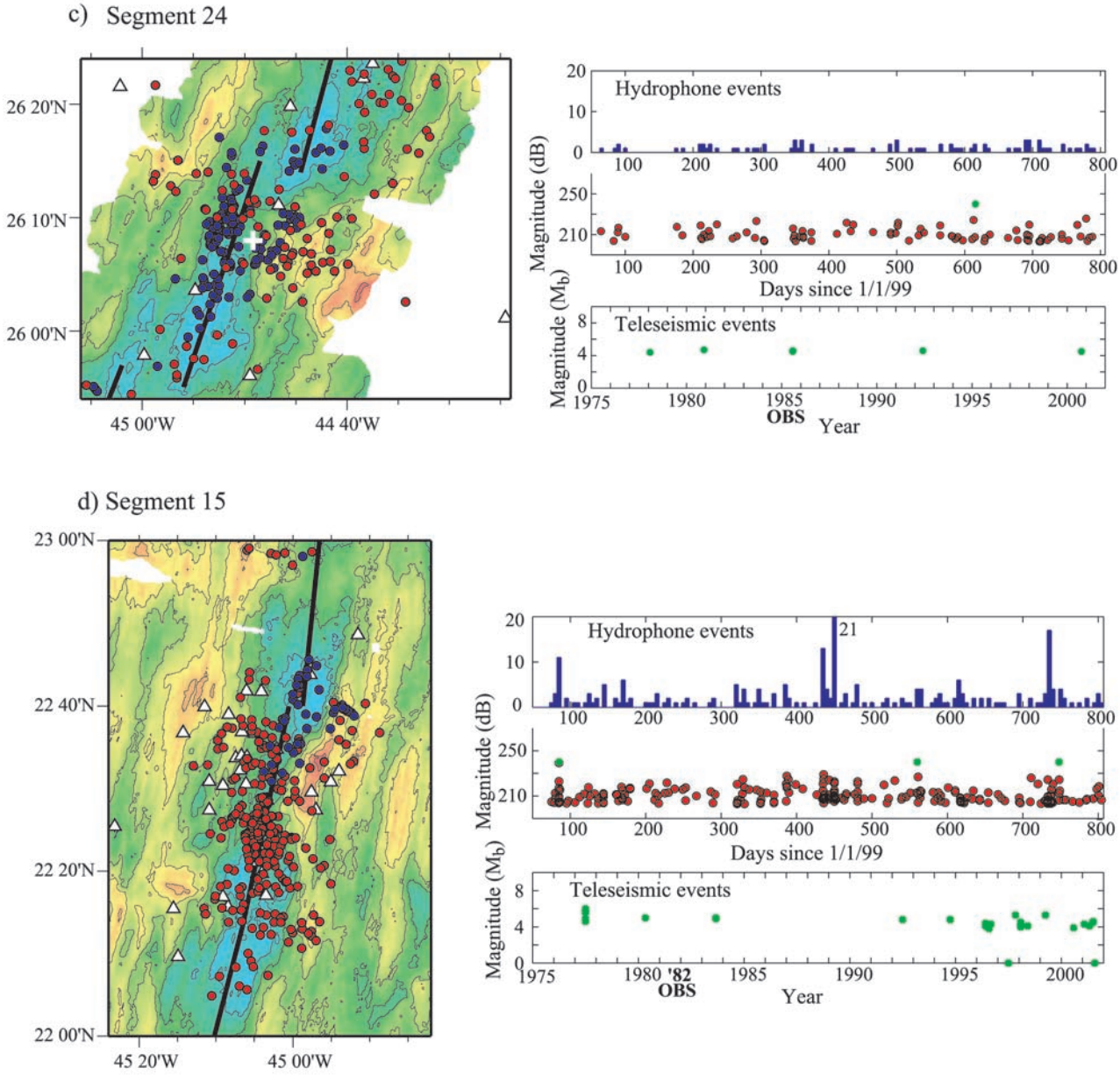

Figure 13. (continued)

intermediate to low levels of hydrophone-recorded activity, and their examples of hot segments (segments 45, 41, and 7) have low levels of activity. Overall, these data suggest that hot segments undergo less tectonic strain than cold segments, based on the seismic activity recorded by the hydrophones.

[49] On the basis of our results for all of the segments in the study area (see Table 3), we suggest that it is segments with standard characteristics (a shallower central region, a corresponding relative minimum in the gravity anomaly, and deeper extremities associated with relative gravity maxima) and a shallow axial depth at center that have low seismic activity. In contrast, segments with a large number of hydrophone-recorded events frequently have nonstandard characteristics and axial depths at segment center in excess of 3700 m (Table 3). In the 15°–35°N region of the MAR, there is a correlation (although not a perfect one) between the axial depths at segment centers and the width and depth of the axial valley: the shallower the axial center depth, the narrower and shallower the axial valley. The shallow axial depths, as argued by *Neumann and Forsyth* [1993], likely represent a combination of hot and thick crust and thinner lithosphere.

[50] We note that a large ΔMBA is not essential for segments to have low levels of hydrophone-recorded activity. The along-axis ΔMBA has often been used to infer magma budget (the amount of melt being supplied to a segment), and to determine its current magmatic or amagmatic state. If ΔMBA simply represents the difference in crustal thickness between a segment center and its ends, it is in fact more equivalent to the degree of magma focusing. For example, segments 7–10 south of the Kane FZ, which

have low levels of hydrophone-recorded activity, have small ΔMBAs and small along axis relief, but they all have shallow axial depths and shallow axial valleys, suggesting relatively thin lithosphere. They may be hot segments with poor magma focusing. In contrast, segments 14, 41 and 45, which also have low levels of activity, have a large ΔMBA, large along-axis relief, and shallow central depths suggesting that they are hot segments with focused melt supply.

[51] Gaps in activity occur predominantly in the center of standard segments with shallow axial depths. More than half of the gaps occur within segments that are long and have large along-axis relief and ΔMBA (e.g., segments 14, 38, 41, and 45 and, to a lesser extent, segment 12, 16, and 29). Gaps also occur in standard segments with shallow axial depths but small ΔMBAs (segments 10, 26, and 28). The only segment with a gap at its center that is not a standard segment is segment 12, which has no clear axial valley. The off axis traces of a wide and migrating discontinuity are observed on both flanks, and immediately to the east of the center is a large, recently constructed volcano [*Gente et al.*, 1995]. Our interpretation is that segment 12 is the locus of a recent large influx of magma that has not yet transformed the discontinuity into a new segment. Thus segment 12 is nonstandard but could have a hot axial thermal regime.

[52] On the basis of the OBS results at segment 45 [*Barclay et al.*, 2001], it is possible to argue that the low levels of hydrophone-recorded activity in segments similar to segment 45 (shallow, large along-axis change in relief and MBA) are due to thin lithosphere, producing earthquakes (tectonic or hydrothermal/volcanic) below the detection limit of the hydrophones and the teleseismic network. The thin lithosphere is a result of higher axial temperatures and focused upwelling generating significant changes in the MBA along the axis. The same can be argued for those segments with gaps that have shallow axial depths but small ΔMBAs (segments 10, 26, and 28), the lithosphere is thin even though magma supply is not focused.

[53] Our preferred interpretation, therefore, would be that local variation in the thickness of the axial lithosphere is the primary control on the level of seismic activity along the 15°–35°N region. A corollary to this interpretation would be that segments with moderate to thin lithosphere tend to present standard characteristics, while segments that are less clearly defined (nonstandard) correspond to portions of the ridge with a thicker lithosphere.

[54] Low hydrophone recorded event rate could also occur in quiescent areas in which stress is accumulating and not being released such as observed in Iceland [e.g., *Arnott and Foulger*, 1994; *Björnsson et al.*, 1977; *Tryggvason*, 1994]. *Björnsson et al.* [1977] proposed that tectonic and volcanic activity in Iceland occurs episodically at intervals of ~100–150 years, each episode lasting only 5–20 years followed by 80–145 years of quiescence. The systematic association of seismic gaps with standard, shallow segments suggests that stress accumulation would likely be a secondary process though, and not responsible for the patterns observed.

8.2. Fifteen-Twenty to Kane Supersegment

[55] In the Fifteen-Twenty to Kane supersegment a majority of the segments (12 of 17) have low normalized numbers of hydrophone-recorded events. All but four of these 12 segments have shallow axial depths (<3700 m, Figure 9) arguing for a hot thermal regime and thin lithosphere beneath them. Since the average depth of the ridge axis in the supersegment is deeper than in the Atlantis to Hayes or in the Hayes to Oceanographer supersegments, the lithosphere in the Fifteen-Twenty to Kane supersegment is not, on average, thinner than further north along the ridge.

Table 5. Cumulative on Offsets for Each Supersegments

Supersegment	Cumulative Length of Offsets, km	Cumulative Length of Offsets per 100 km, km
Fifteen-Twenty to Kane	171.3	18.4
Kane to Atlantis	120.5	15.9
Atlantis to Hayes	75.1	16.4
Hayes to Oceanographer	110.1	47.8

[56] One way to explain the low seismicity level in so many of the segments could be that cooling is reduced at its discontinuities resulting in thinner lithosphere. This would be especially important at discontinuities with small offsets. Table 2 shows that the Fifteen-Twenty to Kane supersegment has zero obliquity, which is defined as the difference between the overall azimuth of the ridge section and the direction perpendicular to average spreading direction. A calculation of the total offset and total offset normalized to a 100 km ridge length for the four supersegments is shown in Table 5. The Fifteen-Twenty to Kane supersegment has a total offset on discontinuities similar to that in the Kane to Atlantis and the Atlantis to Hayes supersegments. At a smaller scale, we find that offset lengths vary within the continuous low-level region containing segments 6–12 and can be large (Table 1). In addition, segments with low levels of activity are adjacent to segments with high levels of activity. All of these argue against offset length playing a major role in controlling hydrophone-recorded event levels in the region.

[57] Cooling might also be reduced at discontinuities that are short lived: a discontinuity that is very young may be seen as made of crust that is less pervasively disrupted by faults, hence lesser hydrothermal cooling. The map of predicted bathymetry [*Smith and Sandwell*, 1997] shows clearly, however, that discontinuities in the Fifteen-Twenty to Kane region are long lived in places, especially those associated with segments 6–9. At this point we do not have an explanation for the large number of segments that exhibit low levels of hydrophone-recorded events in the Fifteen-Twenty to Kane supersegment.

8.3. Controls on High Levels of Hydrophone-Recorded Activity

[58] The correspondence between the level of hydrophone-recorded activity, segment morphology and gravity, and axial depth at the segment center, is not as straightforward for segments with high hydrophone-recorded activity as those with low hydrophone-recorded activity. The conclusion that low levels of hydrophone-recorded activity occur in standard segments with shallow water depths at their centers seems robust. The opposite is not always true, however. Standard segments with shallow water depths at the center do not always exhibit low activity. High hydro-

phone-recorded event activity (>75 events, Figure 7) occurred in 6 of these segments (segments 18, 25, 30, 32, 37, and 40). Four of them (segments 25, 30, 37, and 40) contain regions of near-continuous hydrophone-recorded activity (stripes). High hydrophone-recorded event activity also occurred in five nonstandard segments (segments 3, 13, 15, 27, and 31) with deep axial water depths (>3700 m). All of these five segments have stripes of seismic activity within them. Only segments 18 and 32, which had high event rates, are not classified as stripes. In these segments the events are clustered in time. In segment 18 a large aftershock sequence followed a teleseismic event in the western bounding walls. In segment 32 a large earthquake sequence was located near the southern IC.

[59] The possible causes for high level and persistent hydrophone-recorded activity could include (1) activity related to cooling of a segment; (2) deformation associated with magma movement within the crust; and (3) tectonic deformation. In segment 32 we infer that large volume eruptions have been occurring to build the robust axial volcanic ridge observed on the valley floor, and that a magma reservoir might have existed (or exists) beneath much of the segment to yield the extended flat top of the along axis profile. The ΔMBA suggests that the crustal thickness may vary by as much as 3 km from the end to the center of the segment [*Lin et al.*, 1990]. In contrast, results from the OBS study of *Wolfe et al.* [1995] indicate that that the thickness of the brittle layer, as inferred from microearthquake activity, does not shallow from the southern end of the segment to its center. One way to interpret this is that cooling of the segment is very efficient, and/or that it is occurring at a timescale shorter than that recorded by other segment variables, such as bathymetry or gravity structure. If this is the case then persistent seismic activity in some of the standard, shallow segments may reflect these cooling processes. The seismicity might result from faulting and/or hydrothermal cracking with magnitudes large enough to be detectable by the hydrophones.

[60] Recent studies of the Gakkel ridge in the Arctic Basin have shown that the movement of magma within the crust and eruption of lava can be detected teleseismically at this ultra slow spreading ridge [*Edwards et al.*, 2001; *Tolstoy et al.*, 2001]. It is not known what the seismic characteristics of an eruption at the slow spreading MAR would be, but based on the sizes of the axial volcanic ridges built on the valley floor [*Smith and Cann*, 1999] they might last several years and thus be characterized by persistent seismic activity over a long period of time. We have no additional evidence, however, to suggest that eruptions have occurred during our monitoring period.

[61] Seismic activity at segment 15 was more or less continuous throughout the 2-year recording period with an average rate of 1 event/3 days. In our first paper [*Smith et al.*, 2002] we suggested the possibility that the characteristics of the events in segment 15 may indicate volcanic activity or a response to deformation caused by magma movement at depth. Other evidence from deep-towed camera imagery (our unpublished data), however, suggests that the part of the segment south of the central high has not been volcanically active for some time as sediments cover it. Whether the hydrophone-recorded activity signals a more recent episode of dike injection with or without an associated eruption, or perhaps the beginning of a new episode of magma inflation at this segment is not known. The sharply peaked bathymetric profile suggests though that any magma within the crust would be very limited in extent.

[62] Another possible explanation for the continuous seismicity at segment 15 is related to its similarities to segment 24, which contains the TAG hydrothermal vent field. As discussed above segments 15 and 24 share many characteristics. They both have very small or ambiguous ΔMBAs. Their along-axis profiles are sharply peaked. In addition, in both segments the neovolcanic zone is shifted west away from the northern IC high. They are both nonstandard segments with axial depths >3700 m. The segments are different in that segment 15 has a high number of hydrophone-recorded events while segment 24 has an intermediate number (Table 4). A new interpretation of the TAG segment based on high-resolution magnetic data (H. Schouten and M. Tivey, personal communication) in combination with near bottom side-scan data [*Kleinrock and Humphris*, 1996a] and the results of the microearthquake study [*Kong et al.*, 1992] suggests that the detachment fault associated with the northern IC and the neovolcanic zone may be active at the same time. The high-resolution side-scan data show that the hanging wall of the detachment fault is pervasively cut by faults and cracks and may be broken up in response to faulting events. The persistent activity recorded by the hydrophones at segment 15, therefore, may result from a combination of fracturing of the hanging wall following a faulting event on the detachment fault, renewed hydrothermal circulation within the newly fractured hanging wall and consequent cooling of the inferred low velocity zone underneath the segment center [*Kong et al.*, 1992], and perhaps magmatic/volcanic activity within the neovolcanic zone. Segment 15 may be a snapshot of the TAG segment in a seismogenically active phase. More detailed studies will be needed at segment 15, though, to understand more completely the origin of the seismic activity at this stripe and others.

9. Conclusions

[63] From the spatial and temporal patterns deduced from two years of hydrophone data collected between 15° and 35°N at the MAR we conclude the following:

1. The major proportion of the events located within the array are closely associated with the spreading axis: 88% occur within 20 km of the axis (Figures 4 and 5). This implies that seismogenic faulting does not continue far out on to the flanks of the ridge and that it is not a major process associated with aging of the crust after ~1.5 Myr, at least at the magnitude level detected by the hydrophones. This result is consistent with the results from studies of fault morphology [e.g., *Escartín et al.*, 1999]: there appears to be little, if any, evidence for faulting beyond the crest of the rift mountains (20–40 km from the axis).

2. Four supersegments bounded by the major FZs occur within the array. The lowest number of hydrophone-recorded events (normalized to a 40 km long segment) occurred in the north of the study area in the supersegment between the Hayes and Oceanographer FZs. Since the pattern of teleseismic events is different from the hydro-

phone pattern and appears to change between decades (Table 2), it is difficult to conclude that there is a persistent pattern in seismicity rates between the supersegments.

3. Event activity shows important variations along the ridge axis. The MAR between 15°N and 35°N shows areas with intense and constant seismic activity (seismic stripes) and areas that lack seismicity (seismic gaps). Because of our limited temporal coverage, we are not sure whether this dual expression of seismicity reflects fundamental differences in the long-term behavior of the respective segments or not. Teleseismic events were commonly associated with the regions of stripes. However, it does not appear that the teleseismic events trigger the smaller magnitude activity recorded by the hydrophones. As far as we know, stripes of activity such as these at the MAR are not observed at intermediate or fast spreading ridges, and understanding the controls on these stripes could lead to new insights into spreading processes at slow spreading ridges.

4. In general, regions and segments with low and high levels of seismic activity are observed both in the two years of hydrophone data and 28 years of teleseismic data, indicating that the patterns may be maintained at timescales between a few years and a few decades.

5. The portion of the MAR with well-defined seismic stripes and gaps, the lowest continuous region of low level hydrophone-recorded activity, and the highest percentage of segments with low level hydrophone-recorded activity is the Fifteen-Twenty to Kane supersegment. Table 2 shows that the Fifteen-Twenty to Kane supersegment is similar to other supersegments in its average number of hydrophone-recorded events. At this point we do not have an explanation for its unique pattern of alternating low and high numbers of seismic events.

6. Hydrophone-recorded events seem to concentrate, on average, at the end of segments compared to their centers. This is consistent with the idea that segment ends are colder, have thicker brittle lithosphere, and thus have more frequent and/or larger tectonic earthquakes. In addition, we find that on average more events occurred at ICs than at OCs. ICs are topographically shallower than OCs, though, and events may be steered by the topography, radiating from shallower points. We currently do not know how important topographic steering is and whether this might result in mislocating events from one side of the axis to the other. Taking the data at face value, we observe that for segments with offsets >5 km, 66% of the activity occurred on the IC compared to the OC. This result is consistent with the idea that there is a cross-axis asymmetry in tectonic extension at the ends of slow spreading ridge segments with more extension being accommodated at ICs [e.g., *Escartín and Lin*, 1995; *Severinghaus and Macdonald*, 1988; *Tucholke and Lin*, 1994].

7. There is no simple relationship between individual segment variables (e.g., length or trend of the segment, the maximum offset of the discontinuities that bound the segment, or the contrast in MBA between segment ends and center) and the number of hydrophone-recorded events.

8. There is a general correlation between thermal structure and seismicity. Low and high numbers of hydrophone-recorded events would correspond to thinner (hotter) and thicker (colder) lithosphere, respectively at the ridge axis.

9. Seismicity may reflect thermal structure at the ridge axis at short timescales (decadal or longer), while bathymetry and crustal thickness may integrate this structure over longer periods of time (order of 1 Myr). The lack of a clear correlation between bathymetry and crustal thickness (as a proxy for long-term magmatic state of the axis) and seismicity (as a proxy of the present-day thickness of the brittle lithosphere) may be explained by the differences in the timescales of the processes involved.

[64] **Acknowledgments.** This project was funded by NSF grants OCE-9811575 and OCE-0136808. D.K.S. carried out part of this work at the Laboratoire de Geosciences Marines, with a grant from University of Paris 7. We thank M. Fowler and the captains and crews of the R/V *Ewing*, R/V *Knorr*, and R/V *Atlantis* for their support and hard work during the hydrophone deployment and servicing cruises. We had many fruitful discussions with J. Cann, J. Collins, J. Lin, R. Stephen, B. Tucholke, and C. Williams. IPGP contribution 1854; WHOI contribution 10671.

References

Abercrombie, R. E., and G. Ekström, Earthquake slip on oceanic transform faults, *Nature*, *410*, 74–77, 2001.

Arnott, S. K., and G. R. Foulger, The Krafla spreading segment, Iceland, 2, The accretionary stress cycle and nonshear earthquake focal mechanisms, *J. Geophys. Res.*, *99*, 23,827–23,842, 1994.

Ballard, R. D., and T. H. van Andel, Morphology and tectonics of the inner rift valley at lat. 36°50′N on the Mid-Atlantic Ridge, *Geol. Soc. Am. Bull.*, *88*, 507–530, 1977.

Barclay, A. H., D. R. Toomey, and S. C. Solomon, Seismic structure and crustal magnetism at the Mid-Atlantic Ridge, 35°N, *J. Geophys. Res.*, *103*, 17,827–17,844, 1998.

Barclay, A. H., D. R. Toomey, and S. C. Solomon, Microearthquake characteristics and crustal V_p/V_s structure at the Mid-Atlantic Ridge, 35N, *J. Geophys. Res.*, *106*, 2017–2034, 2001.

Bergman, E. A., and S. C. Solomon, Earthquake swarms on the Mid-Atlantic Ridge: Products of magmatism or extensional tectonics?, *J. Geophys. Res.*, *95*, 4943–4965, 1990.

Bideau, D., R. Hekinian, B. Sichler, E. Gracia, C. Bollinger, M. Constantin, and C. Guivel, Contrasting volcanic-tectonic processes during the past 2 Ma on the Mid-Atlantic Ridge; submersible mapping, petrological and magnetic results at lat. 34°52′N and 33°55′N, *Mar. Geophys. Res.*, *20*, 425–458, 1998.

Björnsson, A., K. Saemundsson, P. Einarsson, E. Tryggvason, and K. Gronvold, Current rifting episode in north Iceland, *Nature*, *266*, 318–323, 1977.

Bohnenstiehl, D. R., M. Tolstoy, D. K. Smith, and C. G. Fox, Earthquake sequences detected using autonomous underwater hydrophone data from the northern Mid-Atlantic Ridge: February 1999–February 2000, *Eos Trans. AGU*, *81*(48), Fall Meet. Suppl., Abstract T51D-13, 2000.

Bohnenstiehl, D. R., M. Tolstoy, R. P. Dziak, C. G. Fox, and D. K. Smith, Aftershock sequences in the mid-ocean ridge environment: An analysis using hydroacoustic data, *Tectonophysics*, *354*, 49–70, 2002.

Brune, J. N., Seismic moment, seismicity, and rate of slip along major fault zones, *J. Geophys. Res.*, *73*, 777–784, 1968.

Cannat, M., C. Rommevaux-Jestin, D. Sauter, C. Deplus, and V. Mendel, Formation off the axial relief at the very slow spreading Southwest Indian Ridge (49° to 69°E), *J. Geophys. Res.*, *104*, 22,825–22,843, 1999.

Cessaro, R. K., and D. M. Hussong, Transform seismicity at the intersection of the Oceangrapher Fracture Zone and the Mid-Atlantic Ridge, *J. Geophys. Res.*, *91*, 4839–4853, 1986.

Collins, M. D., A split-step Pade solution for the parabolic equation method, *J. Acoust. Soc. Am.*, *93*, 1736–1742, 1993.

Collins, M. D., Generalization of the split-step Pade solution, *J. Acoust. Soc. Am.*, *96*, 382–385, 1994.

Detrick, R. S., H. D. Needham, and V. Renard, Gravity anomalies and crustal thickness variations along the Mid-Atlantic Ridge between 33°N and 40°N, *J. Geophys. Res.*, *100*, 3767–3787, 1995.

Dziak, R. P., C. G. Fox, H. Matsumoto, and A. E. Schreiner, The April 1992 Cape Mendocino earthquake sequence: Seismo-acoustic analysis utilizing fixed hydrophone arrays, *Mar. Geophys. Res.*, *19*, 137–162, 1997.

Edwards, M. H., G. J. Kurras, M. Tolstoy, D. R. Bohnenstiehl, B. J. Coakley, and J. R. Cochran, Evidence of recent volcanic activity on the ultraslow-spreading Gakkel ridge, *Nature*, *409*, 808–812, 2001.

Engeln, J. F., D. A. Wiens, and S. Stein, Mechanism and depths of Atlantic transform earthquakes, *J. Geophys. Res.*, *91*, 548–577, 1986.

Escartín, J., and J. Lin, Ridge offsets, normal faulting, and gravity anomalies of slow spreading ridges, *J. Geophys. Res.*, *100*, 6163–6177, 1995.

Escartín, J., P. A. Cowie, R. C. Searle, S. Allerton, N. C. Mitchell, C. J. MacLeod, and A. P. Slootweg, Quantifying tectonic strain and magmatic accretion at a slow spreading ridge segment, Mid-Atlantic Ridge, 29°N, *J. Geophys. Res.*, *104*, 10,421–10,437, 1999.

Fox, C. G., H. Matsumoto, and T.-K. Lau, Monitoring Pacific Ocean seismicity from an autonomous hydrophone array, *J. Geophys. Res.*, *106*, 4183–4206, 2001.

Gente, P., C. Mevel, J. M. Auzende, J. A. Karson, and Y. Fouquet, An example of a recent accretion on the Mid-Atlantic Ridge: The Snake Pit neovolcanic ridge (MARK area, 23°22′N), *Tectonophysics*, *190*, 1–29, 1991.

Gente, P., R. A. Pockalny, C. Durand, C. DePlus, M. Maia, G. Ceuleneer, C. Mével, M. Cannat, and C. Laverne, Characteristics and evolution of the segmentation of the Mid-Atlantic Ridge between 20°N and 24°N during the last 10 million years, *Earth Planet. Sci. Lett.*, *129*, 55–71, 1995.

Heirtzler, J. R., and T. H. van Andel, Project FAMOUS: Its origin, programs, and setting, *Geol. Soc. Am. Bull.*, *88*, 481–487, 1977.

Huang, P. Y., and S. C. Solomon, Centroid depths of mid-ocean ridge earthquakes: Dependence on spreading rate, *J. Geophys. Res.*, *93*, 13,445–13,447, 1988.

Huang, P. Y., S. C. Solomon, E. A. Bergman, and J. L. Nabelek, Focal depths and mechanisms of Mid-Atlantic Ridge earthquakes from body waveform inversion, *J. Geophys. Res.*, *91*, 579–598, 1986.

Karson, J. A., G. Thompson, S. E. Humphris, J. M. Edmond, W. B. Bryan, J. R. Brown, A. T. Winters, R. A. Pockalny, J. F. Casey, A. C. Campbell, G. Klinkhammer, M. R. Palmer, R. J. Kinzler, and M. M. Sulanowska, Along-axis variations in seafloor spreading in the MARK area, *Nature*, *328*, 681–685, 1987.

Kleinrock, M. C., and S. E. Humphris, Structural asymmetry of the TAG rift valley: Evidence from a near-bottom survey for episodic spreading, *Geophys. Res. Lett.*, *23*, 3439–3442, 1996a.

Kleinrock, M. C., and S. E. Humphris, Structural controls on seafloor hydrothermal activity at the TAG active mound, Mid-Atlantic Ridge, *Nature*, *382*, 149–153, 1996b.

Kong, L. S., S. C. Solomon, and G. M. Purdy, Microearthquake characteristics of a mid-ocean ridge along-axis high, *J. Geophys. Res.*, *97*, 1659–1685, 1992.

Lin, J., and E. M. Parmentier, Mechanisms of lithospheric extension at mid-ocean ridges, *Geophys. J.*, *96*, 1–22, 1989.

Lin, J., G. M. Purdy, H. Schouten, J.-C. Sempéré, and C. Zervas, Evidence from gravity data for focused magmatic accretion along the Mid-Atlantic Ridge, *Nature*, *344*, 627–632, 1990.

Murton, B. J., L. J. Redbourn, C. R. German, and E. T. Baker, Sources and fluxes of hydrothermal heat, chemicals and biology within a segment of the Mid-Atlantic Ridge, *Earth Planet. Sci. Lett.*, *171*, 301–317, 1999.

Mutter, J. C., and J. A. Karson, Structural processes at slow-spreading ridges, *Science*, *257*, 627–634, 1992.

Needham, H. D., et al., The crest of the Mid-Atlantic Ridge between 40°N and 15°N: Very broad swath mapping with the EM12 echosounding system, *Eos Trans. AGU*, *72*(44), Fall Meet. Suppl., 470, 1991.

Neumann, G. A., and D. W. Forsyth, The paradox of the axial profile: Isostatic compensation along the axis of the Mid-Atlantic Ridge?, *J. Geophys. Res.*, *98*, 17,891–17,910, 1993.

Patriat, P., C. Depus, C. Rommevaux, H. Sloan, P. Hunter, and H. Brown, Evolution of the segmentation of the Mid-Atlantic Ridge between 28° and 29°N during the last 10 Ma: Preliminary results form the SARA cruise (R/V *Jean Charcot*, May 1990), *Eos Trans. AGU*, *71*, 1629, 1990.

Rabain, A., M. Cannat, J. Escartin, G. Pouliquen, C. Deplus, and C. Rommevaux-Jestin, Focused volcanism and growth of a slow spreading segment (Mid-Atlantic Ridge, 35°N, *Earth Planet. Sci. Lett.*, *185*, 211–224, 2001.

Reinen, L. A., Slip styles in a spring-loader model with a laboratory-derived constitutive law for serpentinite, *Geophys. Res. Lett.*, *27*, 2037–2040, 2000.

Reinen, L. A., J. D. Weeks, and T. E. Tullis, The frictional behavior of lizardite and antigorite serpentinites: Experiments, constitutive models, and implications for natural faults, *Pure Appl. Geophys.*, *143*, 318–358, 1994.

Rommevaux, C., C. Deplus, P. Patriat, and J.-C. Sempéré, Three-dimensional gravity study of the Mid-Atlantic Ridge: Evolution of the segmentation between 28° and 29°N during the last 10 m.y., *J. Geophys. Res.*, *99*, 3015–3029, 1994.

Rona, P. A., and K. G. Speer, An Atlantic hydrothermal plume: Trans-Atlantic Geotraverse (TAG) area, Mid-Atlantic Ridge crest near 26°N, *J. Geophys. Res.*, *94*, 13,879–13,893, 1989.

Rona, P. A., R. N. Harbison, B. G. Bassinger, R. B. Scott, and A. J. Nalwalk, Tectonic fabric and hydrothermal activity of Mid-Atlantic Ridge crest (lat. 26°N), *Geol. Soc. Am. Bull.*, *87*, 661–674, 1976.

Rowlett, H., Seismicity at intersections of spreading centers and transform faults, *J. Geophys. Res.*, *86*, 3815–3820, 1981.

Rowlett, H., and D. W. Forsyth, Recent faulting and microearthquakes at the intersection of the Vema Fracture Zone and the Mid-Atlantic Ridge, *J. Geophys. Res.*, *89*, 6079–6094, 1984.

Schilling, J.-G., G. Thompson, R. Kingsley, and S. Humphris, Hotspot-migrating ridge interaction in the South Atlantic: Geochemical evidence, *Nature*, *313*, 187–191, 1985.

Sempéré, J.-C., G. M. Purdy, and H. Schouten, Segmentation of the Mid-Atlantic Ridge between 24°N and 30°40′N, *Nature*, *344*, 427–431, 1990.

Sempéré, J.-C., J. Lin, H. S. Brown, H. Schouten, and G. M. Purdy, Segmentation and morphotectonic variations along a slow-spreading center: The Mid-Atlantic Ridge (24°00′N–30°40′N), *Mar. Geophys. Res.*, *15*, 153–200, 1993.

Sempéré, J.-C., P. Blondel, A. Briais, T. Fujiwara, L. Géli, N. Isezaki, J. E. Pariso, L. Parson, P. Patriat, and C. Rommevaux, The Mid-Atlantic Ridge between 29°N and 31°30′N in the last 10 Ma, *Earth Planet. Sci. Lett.*, *130*, 45–55, 1995.

Severinghaus, J., and K. C. Macdonald, High inside corners at ridge-transform intersections, *Mar. Geophys. Res.*, *9*, 353–367, 1988.

Shaw, P. R., Ridge segmentation, faulting and crustal thickness in the Atlantic Ocean, *Nature*, *358*, 490–493, 1992.

Shaw, P. R., and J. Lin, Causes and consequences of variations in faulting style at the Mid-Atlantic Ridge, *J. Geophys. Res.*, *98*, 21,839–21,851, 1993.

Slack, P. D., C. G. Fox, and R. P. Dziak, *P* wave detection thresholds, *Pn* velocity estimates, and *T* wave location uncertainty from oceanic hydrophones, *104*, 13,061–13,072, 1999.

Sloan, H., and P. Patriat, Kinematics of the North American-African plate boundary between 28° and 29°N during the last 10 Ma: Evolution of the axial geometry and spreading rate and direction, *Earth Planet. Sci. Lett.*, *113*, 323–341, 1992.

Smith, D. K., and J. R. Cann, The role of seamount volcanism in crustal construction at the Mid-Atlantic Ridge (24°–30°N), *J. Geophys. Res.*, *97*, 1645–1658, 1992.

Smith, D. K., and J. R. Cann, Building the crust at the Mid-Atlantic Ridge, *Nature*, *365*, 707–715, 1993.

Smith, D. K., and J. R. Cann, Constructing the upper crust of the Mid-Atlantic Ridge: A reinterpretation based on the Puna Ridge, Kilauea Volcano, *J. Geophys. Res.*, *104*, 25,379–25,399, 1999.

Smith, D. K., M. Tolstoy, C. G. Fox, D. R. Bohnenstiehl, H. Matsumotu, and M. J. Fowler, Hydroacoustic monitoring of seismicity at the slow-spreading Mid-Atlantic Ridge, *Geophys. Res. Lett.*, *29*(11), 1518, doi:10.1029/2001GL013912, 2002.

Smith, W. H. F., and D. T. Sandwell, Global sea floor topography from satellite altimetry and ship depth soundings, *Science*, *277*, 1956–1962, 1997.

Spencer, S., D. K. Smith, J. R. Cann, J. Lin, and E. McAllister, Structure and stability of non-transform discontinuities on the Mid-Atlantic Ridge between 24°N and 30°N, *Mar. Geophys. Res.*, *19*, 339–362, 1997.

Thibaud, R., P. Gente, and M. Maia, A systematic analysis of the Mid-Atlantic Ridge morphology and gravity between 15°N and 40°N: Constraints of the thermal structure, *J. Geophys. Res.*, *103*, 24,223–24,243, 1998.

Tolstoy, M., D. Bohnenstiehl, M. Edwards, and G. Kurras, The seismic character of volcanic activity at the ultra-slow spreading Gakkel Ridge, *Geology*, submitted, 2001.

Toomey, D. R., S. C. Solomon, G. M. Purdy, and M. H. Murray, Microearthquakes beneath the median valley of the Mid-Atlantic Ridge near 23°N: Hypocenters and focal mechanisms, *J. Geophys. Res.*, *90*, 5443–5458, 1985.

Toomey, D. R., S. C. Solomon, and G. M. Purdy, Microearthquakes beneath the median valley of the Mid-Atlantic Ridge near 23°N: Tomography and tectonics, *J. Geophys. Res.*, *93*, 9093–9112, 1988.

Tryggvason, E., Surface deformation at the Krafla Volcano, north Iceland, 1982–1992, *Bull. Volcanol.*, *56*, 98–107, 1994.

Tucholke, B. E., and J. Lin, A geological model for the structure of ridge segments in slow spreading ocean crust, *J. Geophys. Res.*, *99*, 11,937–11,958, 1994.

Tucholke, B. E., J. Lin, M. A. Tivey, M. C. Kleinrock, T. B. Reed, J. A. Goff, and G. E. Jaroslow, Segmentation and crustal structure of the western Mid-Atlantic Ridge flank, 25°25′–27°10′N and 0–29 m.y., *J. Geophys. Res.*, *102*, 10,203–10,223, 1997.

Utsu, T., Y. Ogata, and R. S. Matsu'ura, The centenary of the Omori formula for the decay law of aftershock activity, *J. Phys. Earth*, *43*, 1–33, 1995.

Wolfe, C. J., E. A. Bergman, and S. C. Solomon, Oceanic transform earthquakes with unusual mechanisms or locations: Relation to fault geometry and state of stress in the adjacent lithosphere, *J. Geophys. Res.*, *98*, 16,187–16,211, 1993.

Wolfe, C. J., G. M. Purdy, D. R. Toomey, and S. C. Solomon, Microearthquake characteristics and crustal velocity structure at 29°N on the Mid-

Atlantic Ridge: The architecture of a slow spreading segment, *J. Geophys. Res.*, *100*, 24,449–24,472, 1995.

S. Bazin, M. Cannat, and J. Escartin, Institut de Physique du Globe de Paris, Tour 14 Case 89, 4 Place Jussieu, F-75252 Paris Cedex 05, France. (bazin@ipgp.jussieu.fr; cannat@ccr.jussieu.fr; escartin@ipgp.jussieu.fr)

D. R. Bohnenstiehl and M. Tolstoy, Lamont-Doherty Earth Observatory, Box 1000, 61 Route 9W, Palisades, NY 10964, USA. (del@ldeo.columbia.edu; tolstoy@ldeo.columbia.edu)

C. G. Fox, National Oceanic and Atmospheric Administration/Pacific Marine Environmental Laboratory, 2115 SE OSU Drive, Newport, OR 97365, USA. (fox@pmel.noaa.gov)

D. K. Smith, Woods Hole Oceanographic Institution, MS 22, Woods Hole, MA 02540, USA. (dsmith@whoi.edu)